Plasma Sources Science and Technology

PAPER

Electron transport and negative streamers in liquid xenon

IOP Publishing Plasma Sources Science and Technology
Plasma Sources Sci. Technol. **28** (2019) 015006 (19pp) https://doi.org/10.1088/1361-6595/aaf968

Electron transport and negative streamers in liquid xenon

I Simonović[1], N A Garland[2], D Bošnjaković[1], Z Lj Petrović[1,3], R D White[2] and S Dujko[1]

[1] Institute of Physics, University of Belgrade, Pregrevica 118, 11080 Belgrade, Serbia
[2] College of Science and Engineering, James Cook University, Townsville, QLD 4811, Australia
[3] Serbian Academy of Sciences and Arts, Knez Mihailova 35, 11000 Belgrade, Serbia

E-mail: sasa.dujko@ipb.ac.rs

Received 17 September 2018, revised 21 November 2018
Accepted for publication 13 December 2018
Published 28 January 2019

Abstract

In this work we investigate electron transport, transition from an electron avalanche into a negative streamer, and propagation of negative streamers in liquid xenon. Our standard Monte Carlo code, initially developed for dilute neutral gases, is generalized and extended to consider the transport processes of electrons in liquids by accounting for the coherent and other liquid scattering effects. The code is validated through a series of benchmark calculations for the Percus–Yevick model, and the results of the simulations agree very well with those predicted by a multi term solution of Boltzmann's equation and other Monte Carlo simulations. Electron transport coefficients, including mean energy, drift velocity, diffusion tensor, and the first Townsend coefficient, are calculated for liquid xenon and compared to the available measurements. It is found that our Monte Carlo method reproduces both the experimental and theoretical drift velocities and characteristic energies very well. In particular, we discuss the occurrence of negative differential conductivity in the E/n_0 profile of the drift velocity by considering the spatially-resolved swarm data and energy distribution functions. Calculated transport coefficients are then used as an input in fluid simulations of negative streamers, which are realized in a 1.5 dimensional setup. Various scenarios of representing the inelastic energy losses in liquid xenon, ranging from the case where the energy losses to electronic excitations are neglected, to the case where some particular excitations are taken into account, and to the case where all electronic excitations are included, are discussed in light of the available spectroscopy and photoconductivity experiments. We focus on the way in which electron transport coefficients and streamer properties are influenced by representation of the inelastic energy losses, highlighting the need for the correct representation of the elementary scattering processes in the modeling of liquid discharges.

Keywords: liquid xenon, electron transport, Monte Carlo, inelastic collisions, negative streamers

1. Introduction

Transport of charged particles in liquids, plasma-liquid interactions and streamer discharges in the liquid phase constitute a growing field of research, which has many important applications [1, 2]. These applications include plasma medicine [3, 4], plasma water purification [5–9], transformer oils [10, 11] and particle detectors [12, 13]. In particular, there is a rich variety of liquid xenon particle detectors [14]. The wide range of existing and potential applications of these detectors includes gamma ray astrophysics [13], particle physics [15] and medical imaging [16], as well as direct dark matter detection [17, 18]. Liquid xenon is a very good detection medium, due to its physical properties [14]. Its high values of density and atomic number make liquid xenon very efficient in stopping penetrating radiation, while a significant abundance of many isotopes, with different values of nuclear spin, enables the study of both spin dependent and spin independent interactions [14]. Further optimization and understanding of such applications is dependent on an accurate knowledge

of the charged particle transport coefficients, streamer properties and the physical processes involved.

In addition to many useful applications, further theoretical and experimental investigation of transport phenomena in liquids would help in the development of insight into various effects, which are relevant for the interaction of charged particles with dense and disordered media [19]. These effects include multiple scattering effects and structure effects, trapping of charged particles in density fluctuations and the solvation of charged particles in polar liquids [19, 20]. As liquid rare gases are the simplest liquids, they are a good starting point for the development of theoretical models of transport and breakdown phenomena in the liquid phase [19].

1.1. A brief overview of electron transport in liquid rare gases

In recent years the modeling of charged particle transport processes in neutral gases has matured and a number of methods to treat this problem have been developed, e.g. various techniques for solving the Boltzmann equation [21], the Monte Carlo method [22] and semi-quantitative momentum transfer theory [21, 23]. For the more general case of the dense gases and liquids, there has been comparatively less investigation. Most investigations in liquid phase have been performed for electron transport in the sub-excitation energy region [19]. Lekner developed an *ab initio* method for determining the effective potential and the corresponding effective cross section for electron scattering on a focus atom in the liquid phase [24]. This effective potential is determined by using the potential of a single atom and the pair correlation function of the liquid. In addition, Cohen and Lekner have shown that the coherent elastic scattering can be represented in the Boltzmann equation by combining the effective cross section for the liquid phase and the static structure factor [25]. By simplifying the arguments of Lekner, Atrazhev and co-workers have shown that the effective cross section for elastic scattering in liquid argon, krypton and xenon are constant in the limit of lower electron energies [26, 27]. This work was extended by using the partial wave method for determining the effective cross sections for electron scattering in liquid argon and liquid xenon [28–31]. Based on these results, they have calculated mobility, mean energy, and characteristic energy of electrons in liquid argon and liquid xenon, in the framework of the Cohen–Lekner theory [30, 31]. The Cohen–Lekner theory was also used in the study of Sakai and co-workers, who have investigated the electron transport in liquid argon, krypton and xenon [32, 33]. In order to improve the agreement between the calculated and measured drift velocities, they have modified the cross section for elastic scattering empirically. In addition, they have demonstrated that the saturation of drift velocity at higher electric fields, which was previously observed in experiments, can be adequately described by including an effective inelastic cross section for vibrational modes. It was argued that these vibrational modes correspond to the change of the translational states of the clusters of atoms. More recently, Boyle *et al* [19, 34] have evaluated the differential cross sections for electron scattering in liquid argon and liquid xenon by solving the Dirac–Fock scattering equations. In these works, Boyle *et al* [19, 34] extended Lekner's theory by considering multipole polarizabilities and non-local treatment of exchange [19, 34]. Transport coefficients have been calculated for electrons using these cross sections as an input into the multi term Boltzmann equation solution, for the lower values of the reduced electric field. It is also worth noting that in order to thermalize electrons to low energies in rare gases (especially those with Ramsauer–Townsend minimum) in the most efficient way and with a small experimental error, it was necessary to perform swarm experiments at higher pressures, where high density effects became observable [35–37]. One of the alternatives to avoid such effects and obtain low-energy cross sections and scattering lengths was to use molecular hydrogen in the mixture at low reduced electric fields, where the unique solution for the rotational energy loss cross sections for hydrogen exists [38].

Theoretical studies of electron transport processes in liquid rare gases, at higher electric fields, have been performed by several authors. In 1976, Atrazhev and co-workers studied the influence of density dependent scattering effects on the Townsend ionization coefficient [39]. The results of this work are two estimates of the first Townsend ionization coefficient, which have been made by considering the two distinctively different representations of energy losses in the electronic excitations. Jones and Kunhardt also studied electron transport in liquid xenon by using Monte Carlo simulations [40]. The semiclassical model used, was previously applied by Kunhardt for studying electron transport in liquid argon [41]. In this work, the interaction of electrons with the liquid is described in the framework of Van Hove's theory [42]. The group at Hokkaido University has also studied ionization in liquid xenon, as well as the electron attachment in the mixtures of liquid argon and electronegative impurities, including O_2, SF_6 and N_2O, using previously developed cross sections [32]. Considerable contributions in this field have been made by Boyle and co-workers who developed the fluid equation based model for electrons and positrons in liquids by utilizing dilute gas phase cross sections together with a structure factor for the medium [43–46].

1.2. Streamers in liquid rare gases

In comparison to gas phase modeling, there are only a few modeling studies of streamer propagation in liquids. Simulations of positive streamers in hydrocarbon liquids using 1.5D classical streamer model have been performed by Naidis and co-workers [10, 47]. Simulations are performed both without formation of expanding gaseous filaments and in conditions when such filaments due to vaporization are formed. Contemporary studies include both the experimental and numerical studies of propagating streamers inside bubbles elongated along the external electric field and compressed bubbles immersed in water [48, 49]. The salient feature of these studies is that transport coefficients of electrons in liquids required for streamer simulations are evaluated approximately, e.g. without taking into account more serious

perturbations to the transport due to the formation of bubbles and clusters.

Numerical modeling of streamer dynamics, in liquid argon and liquid xenon, has been performed by Babaeva and Naidis [50–52]. They have investigated the formation of a positive streamer in a strong non-uniform field and its subsequent propagation in a weak uniform field, by employing a two dimensional fluid model [50, 51]. Among many important points in these papers, it has been shown that the nature of the streamer propagation in the liquid phase is significantly influenced by the electron-ion recombination [50, 51]. In addition, they found that the calculated streamer velocities are of the same order of magnitude as the measured velocity of the breakdown wave in liquid argon [50, 51].

1.3. Motivational factors for this study

One of the most important conclusions from the previous studies of electron transport in atomic liquids is the fact that still there is no consensus on the importance of excitations in the liquid phase. For example, Atrazhev *et al* [39] have shown that if the portion of energy losses due to excitations is assumed to be just the same as in the gas phase, the first Townsend coefficient is underestimated. On the other hand, if the inelastic energy losses are completely neglected then the first Townsend coefficient is overestimated [39]. Along similar lines, Nakamura and co-workers also disregarded the explicit influence of energy losses associated with the electronic excitations in their calculations of transport properties of electrons in the liquid phase [20, 53]. Instead, they have represented the inelastic energy losses by using an effective inelastic cross section, which corresponds to vibrational modes [20, 32, 53]. In 1993, Jones and Kunhardt carried out Monte Carlo simulations in which the inelastic energy losses due to electronic excitations were included [40]. However, in this work it has not been specified which electronic excitations are included in the set of cross sections [40]. Atrazhev *et al* [39] have shown that a different representation of the inelastic energy losses leads to a significant difference in the calculated values of the ionization rate in liquid xenon. Thus, it is clear that a rigorous analysis of the inelastic energy losses in studies of electron transport in liquid rare gases is long overdue and the present study takes the first steps in this direction. We believe that this is of key importance for numerical studies of streamer propagation, since ionization controls the development of a discharge and occurs in both the streamer head and in the streamer channel.

In this work, we investigate how various representations of the inelastic energy losses affect transport properties of electrons and streamer dynamics in liquid xenon. Cross sections for electronic excitations are taken from the set for electron scattering in the gas phase compiled by Hayashi [54]. This set of cross sections yields swarm parameters in good agreement with the available measurements [55]. We identify and consider the following three global scenarios: (i) no electronic excitations, (ii) some electronic excitations are included and some of them are neglected, and (iii) all electronic excitations are included in the modeling. Various representations of inelastic energy losses are first discussed in light of previous spectroscopy and photoconductivity experiments and then are used in Monte Carlo simulations. The calculated values of the first Townsend coefficient in these various cases are compared with respect to the experimental results of Derenzo *et al* [56]. These calculations are augmented by those in which gaseous xenon is scaled up to the liquid density. In addition to the study of transport processes, in this work we investigate the propagation of negative streamers in liquid xenon. The axial profiles of electric field and number density of electrons are calculated in the absence of vaporization and the occurrence of bubbles.

1.4. Organization of the paper

In section 2 we give the details of cross sections for elastic and inelastic scattering of electrons in liquid xenon. We identify and review the four different cases in three global scenarios for representing the inelastic energy losses. In section 3.1 we briefly outline the Monte Carlo method used in the present work and present the results of benchmark calculations for the Percus–Yevick model in section 3.2. In section 3.3 we present the basic elements of a fluid theory used to simulate negative streamers in liquid xenon. In section 4 we present the electron transport coefficients in liquid xenon with particular emphasis on the structure induced negative differential conductivity (NDC). In the same section, we discuss the transition from an avalanche into a streamer and propagation of negative streamers. In section 5 we present our conclusions and recommendations for future work.

2. Cross sections for electron scattering in liquid xenon

In the gas phase, the electron transport can be represented as a series of individual collisions, which are separated by free flights [19]. However, this picture is no longer valid in the liquid phase. Since no particular volume is owned by a single atom, due to small interparticle spacings in liquids, as compared to the range of interaction between electrons and the targets, the potential in which an excess electron is scattered is determined by many surrounding atoms [19, 24]. Namely, it has been shown that the polarization potential of a single atom is significantly screened by polarization potentials of neighboring atoms [19, 24]. Due to this effect, at low energies, the effective potential changes from an attractive long range potential, which corresponds to scattering on an isolated xenon atom, to a repulsive short range potential, which corresponds to scattering in the liquid phase [24, 28]. In addition, electron scattering on a focus atom will be influenced by electrostatic terms and non-local exchange terms of all neighboring atoms [19]. Moreover, the de Broglie wavelengths of excess electrons at thermal energies are larger than the interatomic spacing by several orders of magnitude [19].

This leads to significant coherent scattering effects, for low energy electrons, which make the electron scattering structure dependent and strongly anisotropic [19, 24]. The anisotropy of coherent scattering leads to a difference between the effective mean free paths for the transfer of energy and momentum [24, 57]. It has been shown that the effective mean free path for the transfer of energy is independent of the liquid structure, while the effective mean free path for the transfer of momentum is structure dependent [24, 57]. The coherent scattering effects and the modification of the scattering potential strongly influence the elastic scattering of the lower energy electrons. However, these effects are reduced with an increasing energy becoming negligible for electron energies higher than approximately 10 eV [39, 57]. This is demonstrated by the density independence of the measured drift velocity for swarms of electrons in compressed gases under high electric fields [58, 59].

Excitations in liquid xenon have been investigated in spectroscopy experiments [60–65]. It has been shown that the reflection spectrum of liquid xenon is very similar to the reflection spectrum of solid xenon [60, 61]. In this spectrum, intermediate $n = 1\left[\Gamma\left(\frac{3}{2}\right)\right]$ and $n' = 1\left[\Gamma\left(\frac{1}{2}\right)\right]$ excitons have been observed at 8.2 eV and 9.45 eV, respectively [61–63]. The former has parentage in the excited atomic $6s[3/2]_1$ state, while the latter has parentage in the $6s'[1/2]_1$ state [63]. In addition, a spectral line, which has developed from the two neighboring $5d[3/2]_1$ and $7s[3/2]_1$ states, has been observed at about 10.32 eV [63, 66]. Another spectral line has been observed at 9 eV [61–63]. This line belongs to the $n = 2\left[\Gamma\left(\frac{3}{2}\right)\right]$ Wannier exciton, which does not originate from the states of an isolated atom [61–63]. Since excitons are closely related to the electron band structure, the presence of excitonic lines in the reflection spectrum indicates the existence of the valence band and the conduction band in liquid xenon [66]. In addition, the value of $\Gamma\left(\frac{3}{2}\right)$ band gap has been determined from the corresponding Wannier series [67]. The obtained value of the band gap is 9.22 eV, and it is in excellent agreement with the prediction on the change of the corresponding band gap in the solid phase [66, 67]. This value has been further verified by using the measured photoconductivity threshold in liquid xenon (9.202 eV) and the known difference between the photoconductivity threshold and the $\Gamma\left(\frac{3}{2}\right)$ band gap in the solid xenon (0.013 eV) [67].

Thus, a cross section set for electron scattering in liquid xenon has to include the cross sections for elastic scattering, inelastic energy losses and the interband transitions [40, 41]. We employ four different cases for representing the inelastic energy losses in order to study the influence of the inelastic collisions on the transport properties of electron swarms and the dynamics of negative streamers in liquid xenon. Each of these cases is discussed in light of previous spectroscopy and photoconductivity experiments. Elastic scattering and the interband transitions are represented in the same way in all cases considered.

2.1. Elastic scattering and interband transitions

The elastic scattering of low energy electrons is strongly influenced by the changes in the scattering potential and the coherent scattering effects [19, 24, 26, 34]. Moreover, the effective mean free paths for the transfer of momentum and energy in liquids are different due to a strong anisotropy of coherent scattering [24, 57]. These mean free paths are given by

$$\Lambda_0 = (n_0\sigma_m)^{-1} = \left(n_0 2\pi \int_0^\pi \mathrm{d}\chi \sin\chi(1-\cos\chi)\sigma_{\mathrm{sp}}(\epsilon,\chi)\right)^{-1}, \quad (1)$$

$$\Lambda_1 = (n_0\tilde{\sigma}_m)^{-1} = \left(n_0 2\pi \int_0^\pi \mathrm{d}\chi \sin\chi(1-\cos\chi)\sigma_{\mathrm{sp}}(\epsilon,\chi)S(\Delta k)\right)^{-1}, \quad (2)$$

where n_0 is the liquid number density, $\sigma_{\mathrm{sp}}(\epsilon, \chi)$ is the differential cross section for elastic scattering of an electron on a focus atom in the liquid phase, ϵ is the relative energy in the center of mass frame, χ is the angle through which the relative velocity is changed and $S(\Delta k)$ is the static structure factor, as a function of the transferred momentum. In these equations $\tilde{\sigma}_m$ and σ_m represent the momentum transfer cross sections with and without the structure modification, respectively [57].

As proposed by Tattersall and co-workers, the ratio $\gamma(\epsilon) = \frac{\Lambda_0}{\Lambda_1}$ represents the measure of the anisotropy of coherent scattering [57]. The coherent scattering is modeled as a combination of three distinct effective scattering processes, which give a good representation of the average transfer of momentum and energy [57]. In the first of these processes, represented by the σ_{both} cross section, both energy and momentum are transferred as in an ordinary binary collision [57]. In the second process, represented by the $\sigma_{\mathrm{momentum}}$ cross section, the electron is scattered in a random direction, but the speed of the electron remains unchanged. This leads to a transfer of momentum, without a concomitant transfer of energy [57]. In the third process represented by the σ_{energy} cross section the energy of the electron is reduced as in an ordinary binary collision, but the electron does not change the direction of its motion. This leads to a transfer of energy, which is accompanied by a minimal transfer of momentum [57]. It is important to emphasize that these effective scattering processes do not represent individual microscopic collisions, but rather provide a good representation of the average rates of momentum transfer and energy transfer in structured media [57].

The cross sections for the corresponding effective processes are determined from $\gamma(\epsilon)$ and the momentum transfer cross section, for electron scattering on a focus atom in the liquid phase, $\sigma_m(\epsilon)$ [57]. The values of $\sigma_m(\epsilon)$ and $\gamma(\epsilon)$, which are used in the present work, have been determined by Boyle *et al* [34].

For $\gamma(\epsilon) < 1$ these cross sections are calculated as [57]:

$$\begin{aligned}\sigma_{\text{both}}^{\gamma<1} &= \gamma(\epsilon) \cdot \sigma_m(\epsilon)\\ \sigma_{\text{energy}}^{\gamma<1} &= (1 - \gamma(\epsilon)) \cdot \sigma_m(\epsilon)\\ \sigma_{\text{momentum}}^{\gamma<1} &= 0.\end{aligned} \tag{3}$$

For $\gamma(\epsilon) > 1$, these cross sections are given by [57]

$$\begin{aligned}\sigma_{\text{both}}^{\gamma>1} &= \sigma_m(\epsilon)\\ \sigma_{\text{energy}}^{\gamma>1} &= 0\\ \sigma_{\text{momentum}}^{\gamma>1} &= (\gamma(\epsilon) - 1) \cdot \sigma_m(\epsilon).\end{aligned} \tag{4}$$

We model the elastic scattering by using these effective cross sections, for energies up to approximately 10 eV. At higher energies both σ_{momentum} and σ_{energy} are taken to be negligible, while σ_{both} is approximated by the elastic cross section for electron scattering in the gas phase [68]. This is a good approximation, since both modifications of the scattering potential and the coherent scattering effects are small for high energy electrons [39, 57].

The cross section for interband transitions is approximated by the cross section for the electron impact ionization, from the Hayashi's cross section set, which is shifted towards lower energies. Specifically, the cross section for ionization is shifted by 2.91 eV, so that its threshold is moved to 9.22 eV. This value corresponds to the $\Gamma\left(\frac{3}{2}\right)$ band gap in liquid xenon, which is the energy difference between the uppermost valence band and the bottom of the conduction band [67]. The use of this cross section gives a good energy balance for the interband transitions, since the energy levels of excess electrons in the conduction band can be represented by a continuous energy spectrum, due to a high density of states in the conduction band [41].

We should note that the energy of the bottom of the conduction band in liquid xenon $V_0 = -(0.66 \pm 0.05)$ eV [69, 70] is not explicitly included in our calculations. This is justified since the system is homogeneous and the inclusion of V_0 would be equivalent to introducing a constant electric potential of the entire system, which would not influence the electron dynamics due to the constant value of this potential. It should also be noted that V_0 is implicitly included in the formula for the difference between the value of the ionization potential of an isolated atom and the value of the band gap in the liquid phase [40]. The inclusion of V_0 in calculations is necessary in the case of the gas-liquid interface (and other situations in which the number density of the background atoms is inhomogeneous) since the change of V_0 across the interface produces an effective electric field as shown in the recent study of Garland and co-workers [71]. Thus, in our calculations we can effectively represent discrete energy levels of quasi free electrons in the conduction band which have a minimum of V_0 with a continuous energy spectrum of free electrons which have a minimum of 0 eV.

2.2. Case 1: No electronic excitations

In the first case, the inelastic energy losses are completely neglected. It was shown by Atrazhev *et al* that this approach overestimates the first Townsend coefficient in liquid xenon [39]. However, this case is considered in our study with the aim of establishing the influence of electronic excitations on the first Townsend coefficient. This case will be referred to as case 1.

2.3. Case 2: Only excitations $6s[3/2]_2$ and $6s[3/2]_1$ are included

In our remaining cases inelastic energy losses are taken into account, since it has been shown in experiments that both excitons and perturbed atomic excitations exits in liquid xenon [62, 63]. Moreover, it has been determined that the excitation of these electronic states is the main channel of energy loss of excess electrons in liquid argon, krypton and xenon under the moderate electric fields [72–74]. However, no cross sections for the excitation of these discrete states can be found in the literature. Since intermediate excitons have unique parentage in the excited states of the atom [62, 63, 75], we approximate the cross sections for both intermediate excitons and the perturbed atomic excitations by the cross sections for the corresponding excitations of an isolated atom. The cross sections for excitations, which are used in our work, are those from the Hayashi cross section set for electrons in gaseous xenon [54, 68].

We do not change the values of the thresholds for excitations, since only thresholds for optically allowed excitons are present in the literature [75], while the optically forbidden states have to be included in our model as well. Therefore, it would be somewhat inconsistent to modify the thresholds for the optically allowed transitions, while leaving the thresholds for the optically forbidden transitions unchanged. Moreover, it has been shown that in the reflection spectrum of liquid xenon, there exists an additional line, next to the $n = 1$ $\left[\Gamma\left(\frac{3}{2}\right)\right]$ exciton line [62, 63]. This line corresponds to the perturbed atomic $6s[3/2]_1$ state [62, 63]. It was determined by Laporte *et al* that about 10% of atomic clusters in liquid xenon, near the triple point, will give rise to the perturbed atomic line, instead of the corresponding exciton line [62]. This is caused by the fact that these clusters do not have a sufficient number of atoms for the formation of the exciton inside a volume which corresponds to the exciton radius [62, 63]. Therefore, if one was to construct a model which distinguishes intermediate excitons from the corresponding perturbed atomic states, one would have to know which percentage of atomic clusters give rise to the perturbed atomic lines, instead of the corresponding excitonic lines, for each atomic excitation. In addition, one would have to know the thresholds for all excitons and all perturbed atomic excitations, including the optically forbidden states. This is beyond the scope of our paper, and we model both the intermediate excitons and the perturbed atomic excitations with the corresponding excitations of an isolated atom. However, the difference between these thresholds is less than 5% for all observed excitons [62, 63, 75]. Thus, we anticipate a small error is made by using the thresholds from the gas phase.

We neglect the observed $n = 2\,\Gamma\left(\frac{3}{2}\right)$ Wannier exciton, in all of our cases, since it does not correspond to any individual atomic state. No other Wannier exciton, for $n > 1$, has been identified in the reflection spectra of liquid xenon [61–63, 75]. For simplicity, in the rest of this work the interband transition and the inelastic collisions will be sometimes referred to as ionization and excitations, respectively. Comparing to binary inelastic collisions, these processes are not the same, as every xenon atom is located in a cluster of the surrounding atoms. Thus, atomic excitations are replaced either by excitons or by perturbed atomic excitations, depending on the size of the atomic cluster [62, 63]. Likewise, binary ionization is replaced by the excitation of an electron from the valence band to a quasi free state in the conduction band [66, 67].

In the second case, only excitations with thresholds, which are lower than the threshold of the interband transition, are included in the cross section set. This includes $6s[3/2]_2$ and $6s[3/2]_1$ atomic states. These two excitations correspond to the first two inelastic collisions in the Hayashi's cross section set [54]. The former of this state is optically forbidden, while the latter is optically allowed. Both the $n = 1\left[\Gamma\left(\frac{3}{2}\right)\right]$ exciton, and the corresponding perturbed atomic state, which have been observed in experiment [61–63], have parentage in the second of these excitations.

2.4. Case 3: The first four excitations from the Hayashi's set of cross sections are included

In the previous experimental investigation of photoconductivity in liquid xenon it has been shown that other discrete states should also be included in the set of cross sections. Specifically, a dip has been observed in the photoconductivity spectra of liquid xenon at 9.45 eV [67]. This dip is induced by the competition between continuous band to band transitions and the discrete $n' = 1\left[\Gamma\left(\frac{1}{2}\right)\right]$ exciton [67]. The observed dip in the photoconductivity spectra of liquid xenon indicates that the corresponding discrete state has decay channels alternative to dissociation like luminescence [66]. This indicates that the inelastic energy losses due to this discrete state should be included in the modeling of electron transport in liquid xenon. The $n' = 1\ \Gamma(\frac{1}{2})$ exciton has parentage in the $6s'[1/2]_1$ atomic state [62, 63]. Another atomic excitation exists between $6s[3/2]_1$ and $6s'[1/2]_1$ states [54]. This is the optically forbidden $6s'[1/2]_0$ state. In this case it is important to take into account both $6s'[1/2]_0$ and $6s'[1/2]_1$ states, in addition to the excitations which are included in the second case. The $6s'[1/2]_0$ state corresponds to the third electronic excitation in the set of cross sections developed by Hayashi [54]. The fourth electronic excitation in the Hayashi's cross section set corresponds to a combination of $6s'[1/2]_1$ and $6p[1/2]_1$ states [54]. Thus, we include the first four excitations from the Hayashi's cross section set in our third case. This case will be referred to as case 3.

2.5. Case 4: All electronic excitations from Hayashi's cross section set are included

In the experimental investigation of the photoconductivity spectra of liquid xenon near the triple point, no further structure could be ascertained above 9.45 eV [67], and the photoconductivity spectra has only been shown for energies lower than 10 eV [67]. However, in a latter experimental investigation of the density dependence of the photoconductivity spectra in fluid xenon by Reininger *et al*, two more dips have been observed for densities up to 77.86% of the triple point density [66]. This is the highest density for which results are reported in their study. The first of these dips is at 10.32 eV corresponding to the discrete transition, which is formed from the two neighboring $5d[3/2]_1$ and $7s[3/2]_1$ states [66]. The second dip is caused by the perturbed $5d'[3/2]_1$ atomic state and it is observed at 11.6 eV [66].

Thus, it is clear that the discrete states with energies above 10 eV exist in liquid xenon, since a line at 10.32 eV has been observed in the reflectivity spectra [60, 62, 63]. It is also clear that they cause dips in the photoconductivity in fluid xenon up to densities close to the triple point density [66]. This indicates that these states should be included in the calculation of inelastic energy losses of electrons in fluid xenon. However, we are not certain if these discrete states should be included in the representation of the inelastic energy losses in liquid xenon, or if they dissociate into a quasi-free electron in the conduction band and a quasi-free positive hole in the valence band. The presence of the line at 10.32 eV in the reflection spectrum of liquid xenon [60, 63] seems to indicate that these states have alternative decay channels to dissociation due to luminescence. This means that they also contribute to inelastic energy losses of excess electrons. We are not certain which percentage of these discrete states dissociates into a quasi-free electron and a quasi-free positive hole. This case for representing the inelastic energy losses in liquid xenon is based on the assumption that these discrete states always decay through luminescence, or some other non-dissociative process. Thus, the corresponding excitations fully contribute to the inelastic energy losses of excess electrons.

The atomic $5d[3/2]_1$ state corresponds to the 11th excitation of Hayashi's cross section set, while the $7s[3/2]_1$ state is included in the 12th Hayashi's excitation [54]. The $5d'[3/2]_1$ atomic excitation, which causes a dip in the photoconductivity at 11.6 eV, is not included in Hayashi's cross section set. However, the 14th Hayashi's excitation, which corresponds to $9s[3/2]_2$ state, has a threshold of 11.58 eV, and it gives the effective energy loss for all excitations in this energy range in the gas phase. All other effective excitations, from the Hayashi's set, include contributions from the optically forbidden states. Therefore, we should include these excitations in our model, since the absence of the optically forbidden states in the reflection spectrum does not mean that these states do not contribute to the energy losses of excess electrons. Thus, our fourth case for representing the inelastic

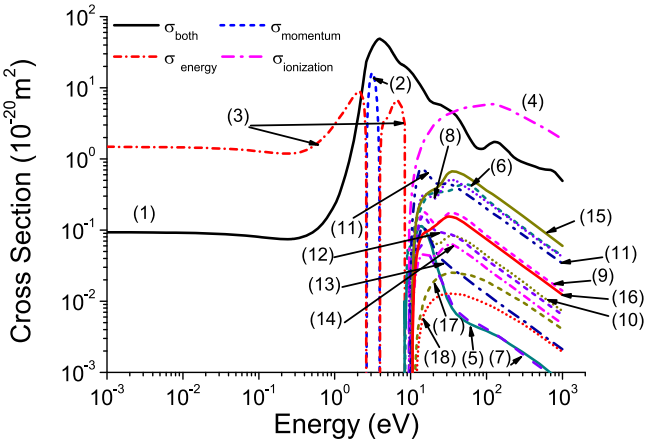

Figure 1. Cross sections for electron scattering in liquid xenon: (1) σ_{both}, (2) σ_{momentum}, (3) σ_{energy}, (4) ionization (the interband transition), effective electronic excitations: (5) $6s[3/2]_2$, (6) $6s[3/2]_1$, (7) $6s'[1/2]_0$, (8) $6s'[1/2]_1$ and $6p[1/2]_1$, (9) $6p[5/2]_2$ and $6p[5/2]_3$, (10) $6p[3/2]_1$ and $6p[3/2]_2$, (11) $5d[1/2]_0$, $5d[1/2]_1$, $6p[1/2]_0$, $5d[7/2]_4$ and $5d[3/2]_2$, (12) $5d[7/2]_3$, (13) $5d[5/2]_2$, (14) $5d[5/2]_3$, (15) $5d[3/2]_1$, (16) $7s[3/2]_2$, $7s[3/2]_1$, $7p[1/2]_1$, $7p[5/2]_2$, $6p'[3/2]_1$, $7p[5/2]_3$, $6d[1/2]_0$, $6d[1/2]_1$, $7p[3/2]_2$ $6d[3/2]_2$, $7p[3/2]_1$, $7p[1/2]_0$, $6d[7/2]_4$, $6d[7/2]_3$, $6p'[3/2]_2$, $6d[5/2]_2$, $6p[1/2]_1$, $6d[5/2]_3$, $6p'[1/2]_0$ and $6d[3/2]_1$, (17) $8s[3/2]_2$ and (18) $9s[3/2]_2$.

energy losses in liquid xenon includes all excitations from Hayashi's cross section set. This case will be referred to as case 4. The cross sections for electron scattering in liquid xenon included in all four cases considered in this work are shown in figure 1.

3. Methods of calculation

3.1. Monte Carlo method

In this work we use the Monte Carlo method to simulate a swarm of electrons in an infinite space, which is filled with a homogeneous background liquid, under the action of a static and uniform electric field. For this purpose, we have modified our existing Monte Carlo code, which has been developed for the study of electron transport in the gas phase [76–78]. Since the dispersion relation for electrons in liquid xenon can be taken to be parabolic and isotropic [40], the influence of the liquid on the electron motion is restricted to scattering events. Thus, the appropriate modification of the scattering dynamics is sufficient to make our Monte Carlo code applicable to the study of electron transport in liquid xenon. This modification has been done by including three effective scattering processes, which represent the coherent scattering of low energy electrons [57]. These scattering processes are described in section 2.1. Our study of the electron transport is performed under the assumption that the density of charged particles is very low (the swarm limit). Thus, we neglect the electron–electron interactions, the space charge effects and collisions with the results of previous collisions (holes and excited states). Therefore, the dynamics of each electron can be followed independently.

The dynamics of an individual electron is determined by the action of the electric field and by collisions between the electron and the atoms of the background liquid. The integral equation for the collisional probability is solved numerically by generating the random numbers from the uniform distribution on the interval (0,1) [76–78].

The type of the next collision is determined by using an additional random number, while taking into account the relative probabilities of all scattering processes for the corresponding value of the electron energy [76–78]. The change of direction of the electron motion after a collision is represented by a pair of angles, i.e. the scattering angle and the azimuthal angle. Isotropic scattering is assumed for all scattering processes, except for the effective scattering process which corresponds to the σ_{energy} cross section. In this process the direction of the electron motion is unchanged by the collision.

After the collision which is represented by the σ_{both} cross section the electron energy is reduced by the factor $\frac{2m\epsilon}{M}(1-\cos\chi)$, where m is the electron mass, M is the mass of a background atom, ϵ is the initial energy of the electron and χ is the scattering angle. The same amount of energy is lost by a low energy electron in the effective scattering process, which is represented by σ_{energy} cross section. When an inelastic collision, or interband transition takes place, the energy of the incident electron is reduced by the energy loss (i.e. the threshold energy) of the corresponding process. After the interband transition, the remaining energy is redistributed between the primary electron and the secondary electron. The fraction of the postcollisional energy, which is obtained by each of these two electrons, is determined by using an additional random number.

In our Monte Carlo code, monomials of coordinates and velocity components of each individual electron are sampled and averaged, over the entire electron ensemble, at discrete sampling times [76–78]. These expressions are used to calculate both bulk and flux transport coefficients of the swarm, with explicit formulas given elsewhere [76–78].

As a large number of electrons must be followed, in order to reduce the statistical fluctuations of the output data, our Monte Carlo simulations are very time consuming. The computational time is particularly large for lower values of reduced electric field, where few inelastic collisions take place. Under these conditions due to a small rate of energy transfer in elastic collisions, the relaxation of energy is inefficient. In order to optimize the computational time and speed of our simulations in the limit of low reduced electric fields, the simulations are performed with a lower number of electrons until the swarm reaches the steady state. After relaxation the swarm is multiplied several times, by cloning each electron, until the desired number of electrons is obtained. When the multiplication is finished all transport properties are calculated from average monomials of both velocities and coordinates. For a more detailed description of our Monte Carlo code, we refer readers to our reviews [76–78].

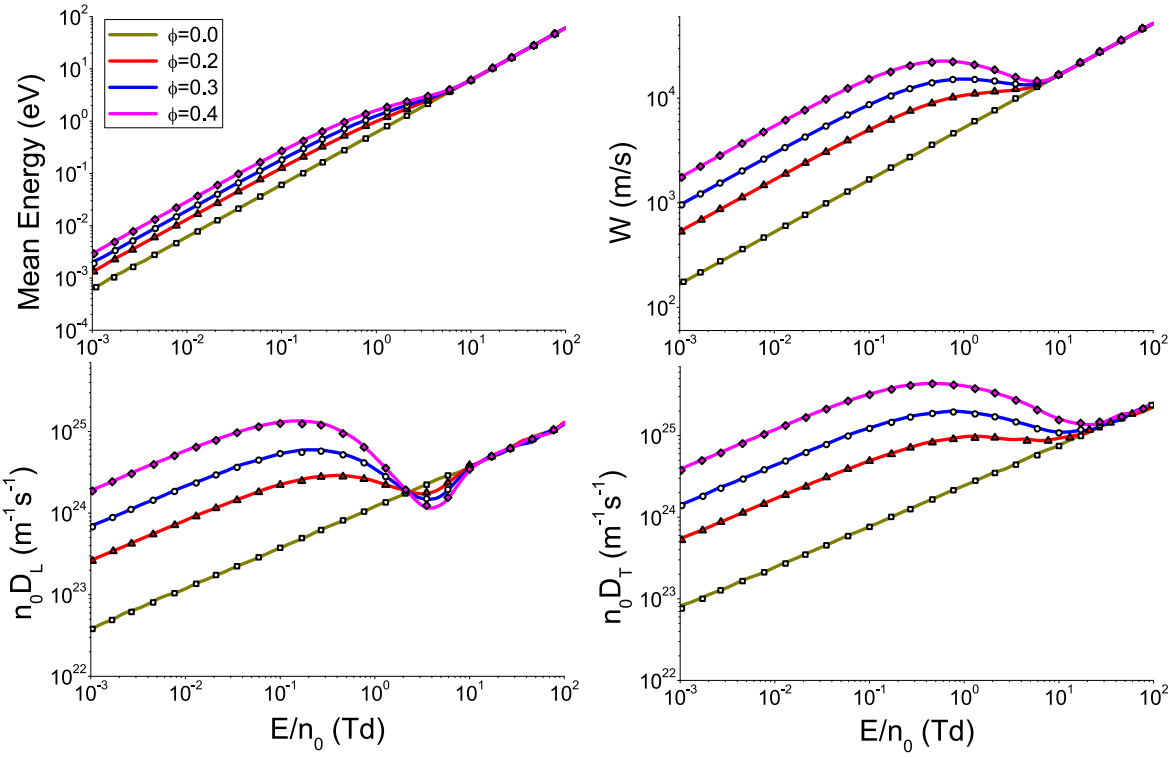

Figure 2. Comparison of our results for mean energy, drift velocity W, longitudinal diffusion coefficient $n_0 D_L$ and transverse diffusion coefficient $n_0 D_T$ of an electron swarm in the Percus–Yevick model liquid, with those of Tattersall *et al* [57]. Transport properties are presented as a function of the reduced electric field E/n_0 and the Percus–Yevick packing ratio ϕ. The present calculations are represented by lines, while the results of Tattersall *et al* [57] are represented by symbols.

3.2. Benchmark calculations

We present our benchmark calculations for the Percus Yevick model liquid, in order to test the implementation of the coherent scattering effects in our Monte Carlo code. The radial pair correlation function, which corresponds to this model, is obtained by applying the Percus Yevick approximation as a closure to the Ornstein–Zernike equation and by representing the interaction between the background molecules by the hard sphere potential [57, 79]. The corresponding static structure factor is obtained as a Fourier transform of this pair correlation function [57]. The modified Verlet and Weis structure factor for the Percus Yevick liquid [80] is used in this work, as in the study of Tattersall *et al* [57]. This structure factor is given by

$$S(\Delta k) = \left(1 + \frac{24\eta}{\Delta k^2}\left[\frac{2}{\Delta k^2}\left(\frac{12\zeta}{\Delta k^2} - \beta\right) + \frac{\sin(\Delta k)}{\Delta k}\left(\psi + 2\beta + 4\zeta - \frac{24\zeta}{\Delta k^2}\right) + \cos(\Delta k)\left(\frac{2}{\Delta k^2}\left(\beta + 6\zeta - \frac{12}{\Delta k^2}\right) - \psi - \beta - \zeta\right)\right]\right)^{-1}, \quad (5)$$

where $\eta = \phi - \frac{\phi^2}{16}$, $\psi = \frac{(1+2\eta)^2}{(1-\eta)^4}$, $\beta = \frac{-6\eta\left(1+\frac{\eta}{2}\right)^2}{(1-\eta)^4}$, and $\zeta = \frac{\eta\psi}{2}$ [57]. The packing ratio ϕ determines the percentage of space which is occupied by the hard spheres. This ratio can be written as $\phi = \frac{4}{3}\pi r^3 n_0$, where r and n_0 are the hard sphere radius and the neutral number density respectively [57].

In figure 2 we show our benchmark results for mean energy, drift velocity and components of the diffusion tensor for electrons in the Percus Yevick liquid, for several values of the packing ratio ϕ. For comparison, the benchmark results of Tattersall *et al* [57] are included in the same figure. Our results are represented by lines, while the results of Tattersall and co-workers are represented by symbols. From a comparison between our results and those predicted by Tattersall *et al* [57], it is evident that the results are consistent for all E/n_0 and ϕ and for all transport coefficients. This suggests that the representation of the coherent scattering effects has been included properly in our Monte Carlo code [81].

In figure 2 we see that all transport properties are distinctively dependent on ϕ for the lower values of E/n_0. Due to coherent scattering effects, all transport properties increase with the increase of ϕ. At the higher values of E/n_0 , however, the strong dependence of transport properties on ϕ is firstly reduced and then entirely removed as the influence of the coherent scattering is negligible for the high energy electrons. On the other hand, the behavior of the longitudinal diffusion coefficient D_L is more complex. We see that D_L increases with the increase of ϕ at low electric fields, but this dependence is inverted for E/n_0 between approximately 2 and 10 Td. The mean energy monotonically increases with the increase of E/n_0 for all values of ϕ. The drift velocity exhibits structure induced NDC, i.e. for E/n_0 approximately between

0.5 and 6 Td and for $\phi \geqslant 0.3$, values of drift velocity decrease as the driving field is increased. The quantitative criterion for the occurrence of the structure induced NDC has been discussed by White and Robson [82]. The decrease of the drift velocity with increasing field can be attributed to the reduction of the coherent scattering effects, which in turn enhance the directional motion of low energy electrons. The reduction of both D_L and D_T with an increasing E/n_0 is also clearly evident. In the limit of the highest E/n_0 considered, all profiles approach to that for $\phi = 0$. It is interesting to note that the values of E/n_0 for this transition decrease with increasing ϕ.

3.3. Fluid model of negative streamers

Our simulations of negative streamers in liquid xenon are performed by using a 1.5 dimensional fluid model [83, 84]. In this model, we assume that the space charge is contained inside a cylinder with radius R_0 and that the charge density varies along the axial direction only. The electron dynamics is described by the continuity equation for the electron number density

$$\frac{\partial n_e(x,\,t)}{\partial t} = \frac{\partial}{\partial x}\left(D_L\frac{\partial n_e(x,\,t)}{\partial x} + W n_e(x,\,t)\mathrm{sgn}(E)\right) + (\nu_i - \beta n_p(x,\,t))n_e(x,\,t), \tag{6}$$

where $n_e(x,\,t)$ and $n_p(x,\,t)$ are the number densities of electrons and positive holes, respectively, which are functions of the coordinate x and time t. In this equation D_L and W are the longitudinal diffusion and the drift velocity respectively, $\mathrm{sgn}(E)$ is the sign function of the electric field E which is oriented along the x-axis, while ν_i and β are the ionization rate and the recombination coefficient, respectively.

Since the hole mobility in liquid xenon is much smaller than the mobility of electrons [85, 86], the positive holes are assumed to be stationary, on the time scales relevant for this study. Thus, the time evolution of the number density of positive holes is described by the number balance equation

$$\frac{\partial n_p(x,\,t)}{\partial t} = (\nu_i - \beta n_p(x,\,t))n_e(x,\,t). \tag{7}$$

The total electric field in the system is represented as the sum of the uniform external field and the electric field due to space charge effects [83, 84]

$$E(x,\,t) = E_0 + \frac{e}{2\varepsilon_0\varepsilon_r}\int_0^l\left(\mathrm{sgn}(x-x') - \frac{x-x'}{\sqrt{(x-x')^2+R_0^2}}\right)(n_p(x',\,t) - n_e(x',\,t))\mathrm{d}x', \tag{8}$$

where E_0 is the external field, e is the elementary charge, ε_0 and ε_r are the vacuum permittivity and the relative permittivity, respectively, and l is the length of the system. The recombination coefficient is given by the scaled Debye formula [50–52]

$$\beta = \xi\beta_{\mathrm{D}} = \xi\frac{4\pi e\mu_e}{\varepsilon_0\varepsilon_r}, \tag{9}$$

where β_{D} is the Debye recombination coefficient, μ_e is the electron mobility, while ξ is the scaling factor which is taken to be 0.1 [10, 50, 51].

The above fluid equations are closed assuming the local field approximation—all transport properties of electrons at a given value of the coordinate x and time t are determined by the local instantaneous electric field, $E(x,\,t)$ and are evaluated from data computed in Monte Carlo simulations. In the numerical implementation of our fluid model, the spatial discretization is performed by using the second order central finite difference, while the fourth order Runge–Kutta method is used for the integration in time. In fluid simulations we follow the transition of an electron avalanche into a negative streamer and its subsequent propagation in liquid medium.

4. Results and discussion

4.1. Transport coefficients for electrons in liquid xenon

In our study of the transport properties of electrons in liquid xenon we cover a range of reduced electric fields between 1×10^{-3} and 2×10^3 Td. The number density of xenon atoms is 1.4×10^{28} m^{-3}, while the temperature of the background liquid is 163 K. For E/n_0 higher than 10 Td, we follow 10^6 electrons during the entire simulation. However, at lower fields our simulations begin with 10^4 electrons and after the relaxation to the steady state the electron swarm is gradually scaled up to 10^6 electrons by cloning each electron at fixed time intervals. The initial velocities of electrons are randomly selected from a Maxwell–Boltzmann velocity distribution which corresponds to a mean energy of 1 eV. All electrons start their trajectories from the same point in space. This point is chosen as the origin of our coordinate system. The cross sections for electron scattering employed in this work are shown in figure 1. The mean energy, drift velocity and diffusion coefficients are shown for cases 1 and 4, as differences between individual cases are too small to be clearly distinguished on logarithmic scale.

4.1.1. Mean swarm energy. The comparison of the mean energies of electron swarms in liquid and gaseous xenon is shown in figure 3. For the lower values of electric fields up to approximately 0.6 Td, the mean energy is higher in liquid xenon than in gaseous xenon due to a significant reduction of the cross section for elastic scattering of the lower energy electrons in the liquid phase. Such behavior is different at higher fields as the mean energy of electrons approaches 1 eV, owing to the fact that the electron scattering in atomic liquids is similar to the scattering in dilute gases for the electron energies higher than 1 eV [19, 34]. The mean energy is lower in the liquid phase than in the gas phase for E/n_0 between approximately 0.6 and 350 Td. At the lower edge of this field region, the difference between the mean

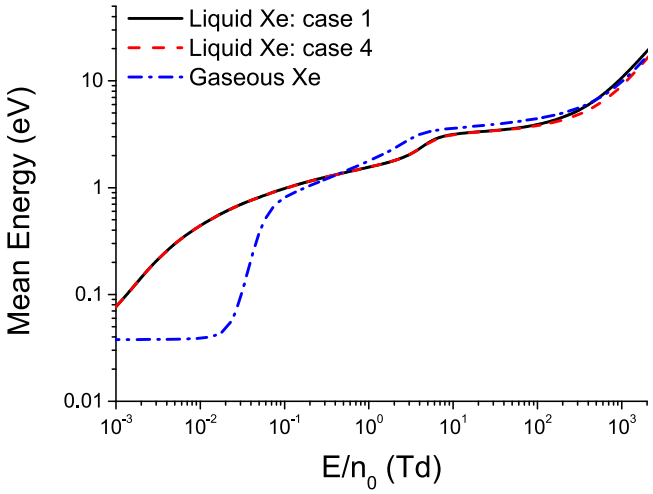

Figure 3. Comparison of the mean energies of electrons in gaseous and liquid xenon. The values of mean energy in liquid xenon, determined by employing two different methods for representing the inelastic energy losses, are shown. In the first case all excitations are neglected, while in the fourth case all excitations from Hayashi's cross section set for electron scattering in gaseous xenon [54, 68] are included.

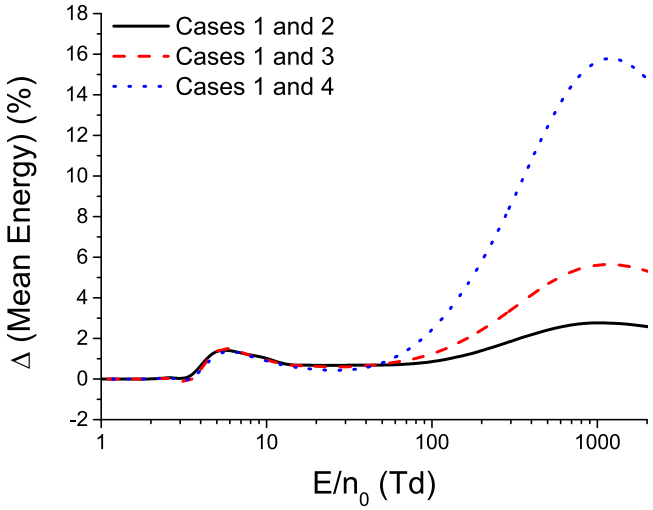

Figure 4. Percentage difference between the values of mean energy, for electrons in liquid xenon, which are determined by using different representations of the inelastic energy losses. All excitations are neglected in the first case. In the second and the third cases only the first two ($6s[3/2]_2$ and $6s[3/2]_1$) and the first four ($6s[3/2]_2$, $6s[3/2]_1$, $6s'[1/2]_0$ and an effective excitation which represents both $6s'[1/2]_1$ and $6p[1/2]_1$) excitations from the cross section set of Hayashi [54, 68] are included. All excitations from the cross section set of Hayashi are included in the fourth case.

energies in gaseous and liquid xenon can be attributed to the greater amount of energy losses in elastic collisions in the liquid phase in the energy region between approximately 0.4 and 10 eV [34]. This is represented by the combined effect of the scattering processes which correspond to σ_{both} and σ_{energy} cross sections. For E/n_0 between approximately 3 and 350 Td this energy difference is caused by the intensive ionization cooling in the liquid phase. Ionization

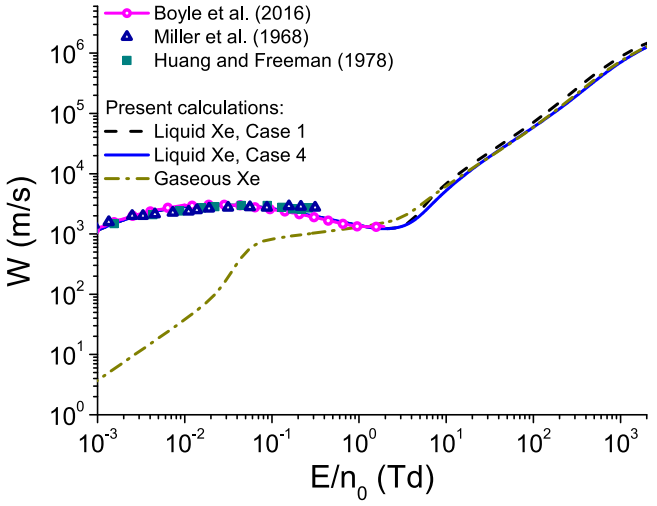

Figure 5. Comparison of the measured drift velocities in liquid xenon (Miller *et al* [88] and Huang and Freeman [89]) with the theoretical calculations. The theoretically determined drift velocities in liquid xenon include those of Boyle *et al* [34] as well as the bulk drift velocities calculated in this study by employing two different methods for representing the inelastic energy losses. The bulk drift velocity of electrons in gaseous xenon is also shown in this figure for comparison.

cooling of an electron swarm in gases has been discussed by Robson and Ness [87]. At higher fields the mean energy in the first case for representing excitations in liquid xenon is slightly higher, while the mean energy in the fourth case is slightly lower, than the mean energy in the gas phase.

In figure 4 we show the percentage difference between the calculated mean energy, assuming the first and the remaining three cases. This difference is negligible for E/n_0 less than 2 Td as electrons undergo elastic collisions only. For E/n_0 higher than 2 Td the mean energy reaches the highest value in the first case due to the absence of inelastic energy losses. The percentage differences between the values of mean energy in the first case and the remaining three cases reach two local maximums at about 5 and 1000 Td, and a local minimum around 27 Td. The first local maximum occurs due to the absence of inelastic energy losses, lower than the threshold energy for ionization, in the first case. The local minimum appears in the field region in which the energy losses due to ionization become comparable to the inelastic energy losses. For E/n_0 higher than 50 Td, the mean energy decreases with the increase of the number of excitations which are included in the model. This is a consequence of a significant competition between ionization and excitations with thresholds higher than 9.22 eV in this field region. The percentage difference between the mean energy in the first case and the remaining cases never exceeds 3%, 6% and 16% for the second, third and fourth cases respectively. Even though the percentage difference between the values of mean energy in various cases decreases for E/n_0 greater than 1000 Td, the absolute difference continues to rise monotonically in the entire field region covered in this study. For the values of E/n_0 lower than 50 Td, these differences are

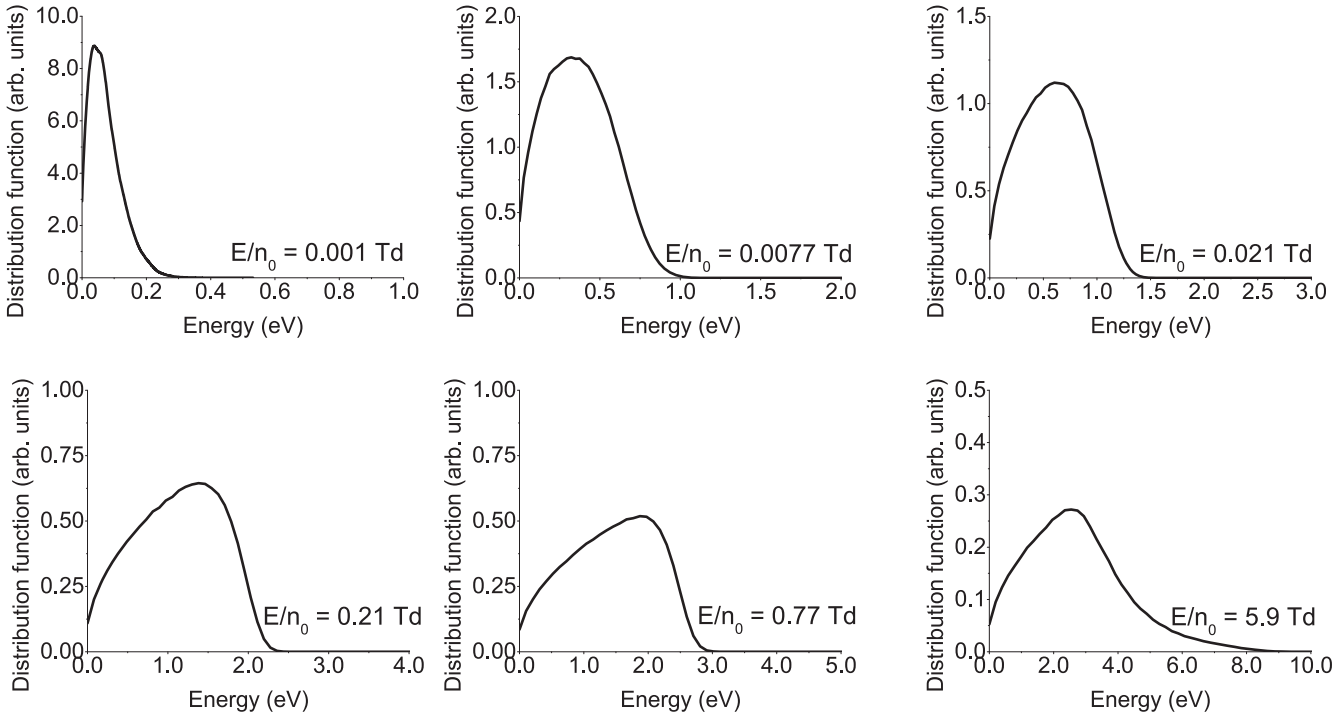

Figure 6. Energy distribution function of the electrons for various E/n_0 as indicated on the graph. Calculations are performed assuming the case 2 where excitations $6s[3/2]_2$ and $6s[3/2]_1$ from the set of cross sections developed by Hayashi are included.

very small and are close to the statistical uncertainty of the Monte Carlo simulations.

4.1.2. Drift velocity and NDC. In figure 5 we show bulk drift velocities assuming the first and the fourth cases for representing the inelastic energy losses as a function of E/n_0. For comparison, the theoretical [34] and experimental [88, 89] drift velocities in liquid xenon determined by previous authors are displayed in the same figure, along with the bulk velocity in gaseous xenon. For the values of E/n_0 lower than 1 Td, the drift velocity in the liquid phase exceeds the drift velocity in the gas phase. This is a consequence of the significant reduction of the rate for momentum transfer of the lower energy electrons in liquid xenon due to the modifications of the scattering potential and the coherent scattering effects. The lowering of the rate for momentum transfer enables the electric field to accelerate electrons more efficiently in liquid xenon than in the gas phase, which leads to a significant enhancement of the drift velocity compared to the gaseous xenon. However, this effect is reduced at higher fields as the scattering of a high energy electron on a xenon atom is weakly perturbed by the surrounding liquid. Thus, for the values of E/n_0 between approximately 0.02 and 2 Td the drift velocity in liquid xenon decreases with increasing field, until it reaches the values that are close to the drift velocity in gaseous xenon. The reduction of the drift velocity with increasing E/n_0 is a phenomenon that is well known as NDC [90–92]. While this phenomenon is caused by inelastic and non-conservative collisions in various gases [90, 92], the NDC observed in liquid argon and liquid xenon is entirely structure induced phenomenon [19, 34, 82]. The quantitative criterion for the occurrence of the structure induced NDC has been discussed by White and Robson [82]. At the end of the field region, which corresponds to NDC, the drift velocity in gaseous xenon slightly exceeds the drift velocity in liquid xenon. For the values of E/n_0 higher than 10 Td the bulk drift velocity in the first case exceeds the bulk drift velocities in all other cases as well as the bulk drift velocity in the gas phase due to the strongest explicit effects of ionization in this case.

In order to understand the occurrence of NDC in liquid xenon at low electric fields, in figure 6 we show the energy distribution functions for a few values of E/n_0. Results are presented for the case two only, as the rate coefficients for those inelastic processes excluded in this case are negligible over the range of reduced electric fields considered. At low electric fields, up to approximately 0.008 Td, the majority of electrons have energies below approximately 0.7 eV. The cross section for momentum transfer is very small over the range of energies less than 0.7 eV and hence the drift velocity in liquid xenon is much greater than in the gas phase. However, for E/n_0 greater than approximately 0.02 Td (at this particular value of E/n_0 NDC begins to develop) a large fraction of electrons have energies between approximately 0.7 and 2 eV. There is a rapid rise in both σ_{both} and σ_{energy} with increasing energy in this region. As a consequence, these two cross sections quickly approach the cross section for elastic collisions in the gas phase. For E/n_0 between 0.2 and 1 Td the majority of the high energy electrons have energies between 1.5 and 3 eV where the cross sections σ_{both} and σ_{momentum} increase rapidly and approach their maximal values. The rapid rise of both σ_{both} and σ_{momentum} leads to a decrease of the drift velocity with increasing E/n_0. For E/n_0 higher than approximately 5 Td a large fraction of electrons have energies

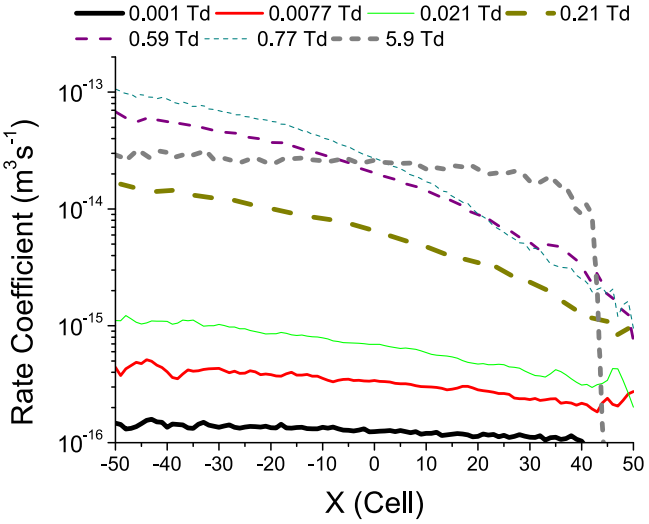

Figure 7. Spatially-resolved rate coefficient for the σ_{both}. Calculations are performed assuming the case 2 where excitations $6s[3/2]_2$ and $6s[3/2]_1$ from the set of cross sections developed by Hayashi are included.

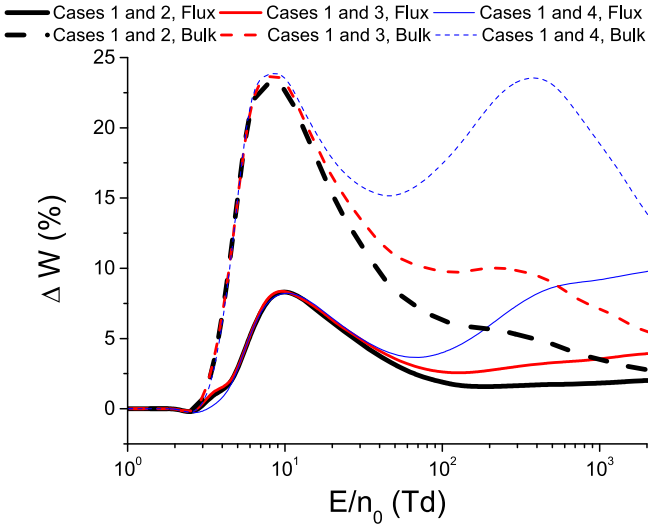

Figure 8. Percentege difference between the values of drift velocities, for electrons in liquid xenon, which are determined by using different methods for representing the inelastic energy losses. These methods are described in the caption of figure 4. Flux and bulk results are represented by solid lines and dashed lines, respectively.

higher than approximately 4 eV, and at these energies the cross section for elastic scattering rapidly drops off with an increase of electron energy. In this range of fields, the drift velocity monotonically increases with E/n_0.

We may also observe that over the range of E/n_0, where the structure induced NDC occurs, the high-energy tail of the distribution function quickly drops off with increasing energy. This is caused due to rapid increase of energy transfer associated with the σ_{both} and σ_{energy}. For E/n_0 lower than approximately 0.008 Td and higher than approximately 4 Td, the high-energy tail of the distribution function drops off more slowly.

In figure 7 we show the spatially-resolved rate coefficient for the σ_{both}. In order to sample spatially-resolved rate coefficients we have divided the real space into cells. The space is divided uniformly into 100 cells in such a way that cells indexed by $(-50, +50)$ correspond to the real coordinates $(x_{\text{cm}} \pm 3\sigma)$, where x_{cm} is the coordinate of the center of mass of the swarm, and the σ is the standard deviation of the x-coordinate of the electrons [93]. Comparing the leading and trailing edges of the swarm, this property is higher at the leading edge where the average energy of the electrons is always greater than at the trailing edge. The slope of the spatially-resolved rate coefficient is the largest over the range of E/n_0 where NDC occurs. Moreover, we observe that the maximal values of this property at the leading edge of the swarm are higher for 0.59 and 0.77 Td than for a higher value of 5.9 Td. A similar behavior is observed for the spatially-resolved rate coefficient for the σ_{momentum}.

The drift velocity calculated in our study is in an excellent agreement with the theoretical results of Boyle *et al* [34]. Our values of the drift velocity are close to those predicted in the experiments of Miller *et al* and Huang and Freeman [88, 89]. However, while most theoretical calculations of the drift velocity predict a structure induced NDC, this effect has not been observed in the experiments. In the field region which corresponds to the onset of the structure induced NDC of the theoretically determined drift velocity, the experimental drift velocity saturates with increasing field. At higher fields, no experimental results are available.

This discrepancy between theoretical and experimental results has been attributed by Sakai *et al* [32] to the presence of additional channels of energy loss in liquids, which are not included in the existing theoretical models. These energy losses correspond to the changes in the translational states of pairs and triplets of xenon atoms upon the electron impact, and they occur for energies much lower than the first threshold for excitations [20, 32]. Sakai and co-workers have empirically derived the sets of cross sections for electron scattering in liquid argon, krypton and xenon [32] which include effective cross sections for representing these additional energy losses. However, an alternative explanation for this discrepancy between theory and experiment could be the presence of molecular impurities in the liquid rare gases used in the experiments. Indeed, it has been shown by Sakai *et al* [32] that even a small amount of molecular impurities in liquefied rare gases leads to a significant enhancement of the electron drift velocity. It might also be the case that the structure induced NDC would be observed in the profiles of the experimentally determined drift velocity at higher electric fields. Further experimental and theoretical investigations are required for the resolving this discrepancy. Thus, the measurement of the drift velocity of electrons in liquid xenon at higher electric fields is of a great importance. In any case, we do not include the effective cross section developed by Sakai *et al* [32] in our model, as it is not adjusted to our cross section for elastic scattering.

In figure 8 we show the percentage difference between the calculated drift velocity assuming the first and the remaining three cases. The flux drift velocity increases with the decrease of the number of excitations, which are

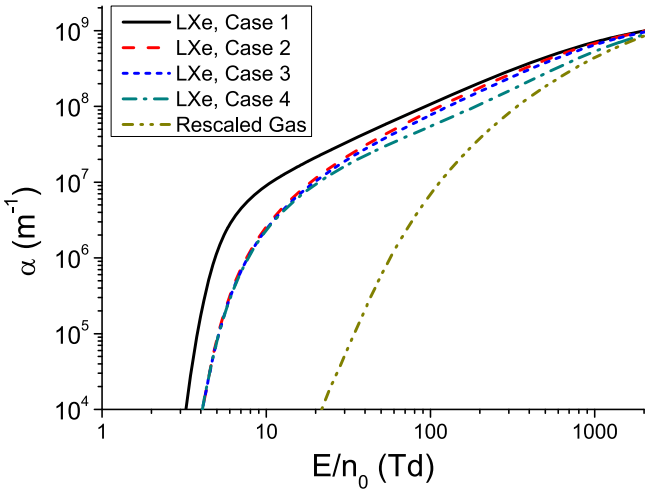

Figure 9. Variation of the first Townsend coefficient with E/n_0 for electrons in liquid xenon. Calculations are performed by assuming all four different methods for representing the inelastic energy losses. These methods are described in the caption of figure 4. The first Townsend coefficient for gaseous xenon, which is scaled up to liquid density is also shown, for comparison.

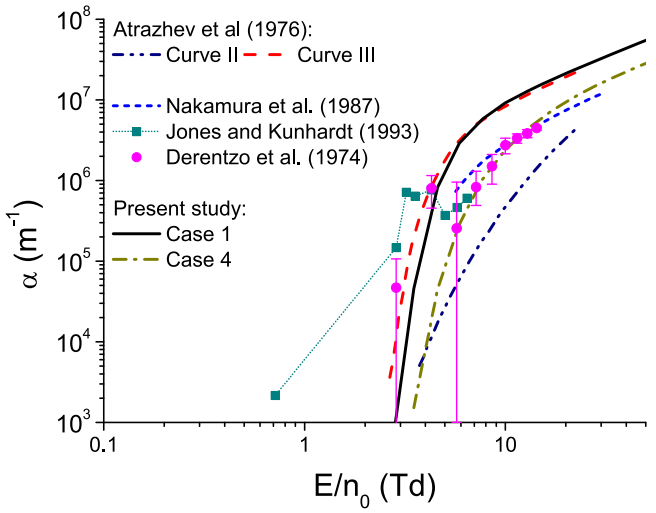

Figure 10. Comparison between the theoretical calculations of the first Townsend coefficient α determined in this study and the results of previous authors. These results include the measurements of Derenzo *et al* [56] and calculations of Atrazhev *et al* [39], Jones and Kunhardt [40] and Nakamura *et al* [53].

considered in the model. This is caused by the lowering of the chaotic component of the electron velocity due to the increase of the ionization cooling with the reduction of the inelastic energy losses [87]. In the case of the bulk drift velocity, this increase is even more pronounced due to the explicit effects of ionization. The percentage difference between drift velocities determined in the first case and the remaining three cases has a local maximum at about 8 Td, as the relative difference between rates for ionization has the highest values at low electric fields. This local maximum has a value of about 8% and 24% for flux and bulk drift velocity, respectively. For E/n_0 higher than 100 Td, the percentage difference between flux drift velocities in the first case and the last two cases rises due to increasing rates for inelastic collisions with thresholds higher than 9.22 eV in this field region. The percentage difference between the corresponding bulk drift velocities reaches another local maximum at about 200 Td and 400 Td for the third and the fourth cases respectively. Although the percentage difference between bulk drift velocities in different cases decreases after the last local maximum, the absolute difference monotonically increases in the entire field region below 2000 Td.

4.1.3. First Townsend coefficient. The first Townsend coefficient expresses the number of ion pairs generated by an electron per unit length. It is equal to the ionization collision frequency divided by the electron drift velocity. Our calculations of the first Townsend coefficient α determined by using different representations of the inelastic energy losses in liquid xenon are shown in figure 9. The first Townsend coefficient in gaseous xenon is scaled up to the liquid density and displayed in the same figure for comparison. It can be seen that α monotonically increases with increasing field in all four cases for representing the inelastic energy losses. We also observe that α is reduced with increasing number of included excitations. In the first case, where all excitations are neglected, the coefficient α overestimates those calculated in the remaining three cases over the range of E/n_0 considered. While the absolute difference between the first Townsend coefficient in the first case and the remaining cases increases over the entire E/n_0 range covered in this study, the relative difference has the highest values at E/n_0 lower than approximately 20 Td. For E/n_0 greater than 20 Td the ionization rate coefficient in the fourth case, where all excitations are included, becomes significantly lower than the corresponding rate coefficients in the other three cases. This is a consequence of the increasing inelastic energy losses which have thresholds higher than 9.22 eV in this case.

The first Townsend coefficient in liquid xenon is much higher than the rescaled coefficient in gaseous xenon for E/n_0 lower than 100 Td. In the limit of the highest E/n_0 considered in the present work, however, we observe that the deviations between the ionization coefficients in liquid and rescaled gas are significantly reduced. One of the main reasons for the significant difference between the rate coefficients for ionization in the scaled gaseous xenon and liquid xenon is the reduction of the threshold for ionization in the liquid phase. An electron in gaseous xenon can undergo ionization only at energies higher than 12.13 eV. Moreover, it can lose a significant amount of energy in a wide range of inelastic scattering processes at energies lower than the threshold energy for ionization. However, in liquid xenon any electron with the energy higher than 9.22 eV can excite an electron from the valence band to the conduction band. Furthermore, there is a far lower number of inelastic scattering processes with thresholds which are lower than the threshold for ionization in the liquid phase compared to the gas phase.

In figure 10 we show the first Townsend coefficient measured by Derenzo *et al* [56] along with the theoretical results obtained by previous authors [39, 40, 53]. The values

of the first Townsend coefficient determined in this study by assuming the first and the fourth cases for representing the inelastic collisions are displayed in the same figure for comparison. The experimental results of Derenzo *et al* [56] are significantly higher than the values of α for electrons in gaseous xenon which are scaled to liquid density. An unusual feature of the first Townsend coefficient measured by Derenzo and co-workers is a non-monotonous behavior with the increase of the reduced electric field. However, this non-monotonicity is not outside the range of experimental uncertainty.

The two sets of results determined by Atrazhev *et al* [39] are calculated by assuming two different methods for representing the inelastic energy losses. The values of α represented by curve II are determined under the assumption that the percentage of inelastic energy losses in the liquid phase are just the same as in the gas phase [39]. This curve is significantly below all other curves presented in this figure. The underestimation of α in curve II demonstrates the significant reduction of the inelastic energy losses in liquid xenon compared to gaseous xenon as discussed by Atrazhev *et al* [39]. The values of α represented by curve III are determined by completely neglecting the inelastic energy losses in liquid xenon. This curve is in the best agreement with the first two experimental points of Derenzo *et al* [56] and with our case 1. The first Townsend coefficient determined by Jones and Kunhardt [40] is the only present theoretical result which predicts the non-monotonic behavior of α and it is in a good agreement with the first four experimental points of Derenzo *et al* [56]. However the values of α at higher fields are not shown in their work. The results of Nakamura *et al* [53] agree very well with the last segment of experimental points of Derenzo *et al* [56], while the values at lower fields are not displayed in their paper.

While our case 1 for representing the inelastic energy losses is in the best agreement with the first two experimental points of Derenzo *et al* [56], all other experimental points are in an excellent agreement with our remaining three cases. No experimental data are present in the field range in which there is a significant difference between our last three cases for representing the inelastic collisions in liquid xenon. However, the last two experimental points of Derenzo *et al* [56] are in a slightly better agreement with our fourth case than with the remaining cases.

A possible explanation for the high values of the first two experimental points determined by Derenzo *et al* [56] is the presence of another mechanism for populating the conduction band in liquid xenon, which is more significant than electron impact ionization at low electric fields. One example of such a mechanism is the dissociation of high order Wannier excitons ($n > 1$) due to scattering on the walls of the system, or under the influence of some other perturbation. Another possible explanation is the reduction of the inelastic energy losses at energies lower than 9.22 eV due to some other effects, which are not included in our model.

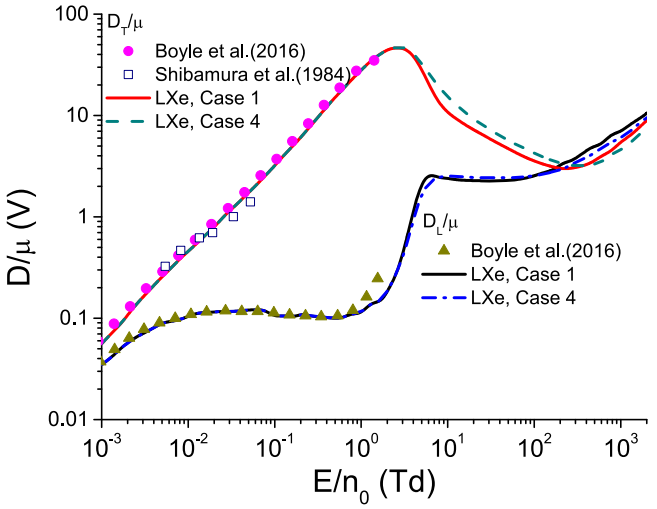

Figure 11. Comparison between the present calculations and those predicted by a multi term solution of the Boltzmann equation (Boyle *et al* [34]) and experimental measurements (Shibamura *et al* [94]) for the bulk values of D_L/μ and D_T/μ. Our results are evaluated by assuming the cases 1 and 4.

4.1.4. Longitudinal and transverse diffusion coefficients. In figure 11 we show the variation of D_L/μ and D_T/μ with E/n_0 assuming the first and the fourth cases for representing the inelastic collisions in liquid xenon. The calculated values of these quantities obtained by Boyle *et al* [34] are also displayed in the same figure for comparison, along with the characteristic energy measured by Shibamura *et al* [94]. Here D_L and D_T denote the longitudinal and the transverse components of the bulk diffusion tensor, while μ is the bulk mobility of electrons. The characteristic energy D_T/μ initially increases with increasing E/n_0, reaching a local peak around 2 Td, and then starts to decrease with E/n_0. For E/n_0 higher than approximately 300 Td, we see that D_T/μ again increases with E/n_0. The E/n_0 dependence of D_L/μ is more complicated. First, there is a region of slow rise of D_L/μ with increasing E/n_0 due to a reduction of the momentum transfer of the lower energy electrons in liquid xenon. Second, there is a region of slow decrease for E/n_0 between approximately 0.05 and 0.4 Td, and then for E/n_0 up to approximately 6 Td there is again a region of rapid rise. Between approximately 6 and 30 Td D_L/μ is reduced as the inelastic collisions start to exert their influence on the swarm. Finally, D_L/μ rises again as the electrons start to rapidly gain energy from the electric field. The complex behavior of D_L/μ in liquid xenon reflects the high sensitivity of this property with respect to the details of cross sections.

We also observe that D_L/μ agree very well with the results of Boyle *et al* [34] for E/n_0 lower than 0.7 Td. However, our results are lower than those of Boyle and co-workers at higher electric fields. The discrepancy can be attributed to the difference in the employed cross sections for the electron scattering, as Boyle and coworkers have neglected the inelastic collisions in their study. As the mean energy of electrons is around 1.8 eV at 1 Td, the most energetic electrons have enough energy to undergo inelastic collisions. The present calculations

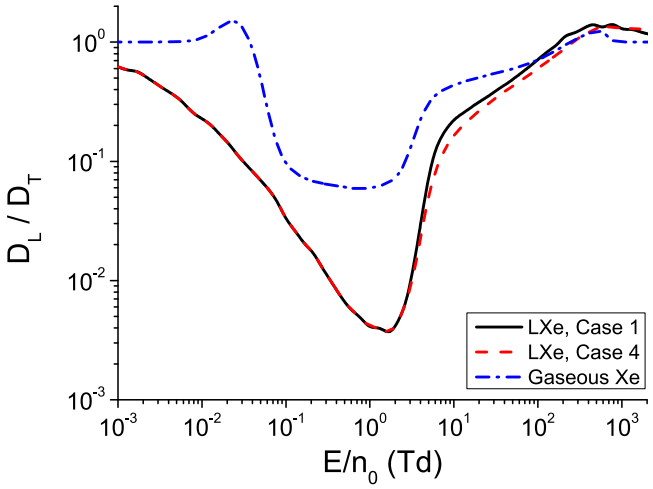

Figure 12. Comparison of the ratios between the bulk longitudinal diffusion and the bulk transversal diffusion in liquid xenon assuming cases 1 and 4 and the same ratio in gaseous xenon. These cases are described in the caption of figure 3.

of D_T/μ are in a good agreement with those predicted by Boyle *et al* [34] and Shibamura *et al* [94].

In figure 12 we show the ratio D_L/D_T for electrons in liquid xenon assuming the first and the fourth cases for representing the inelastic energy losses. The values of D_L/D_T for electrons in gaseous xenon are shown in the same figure for comparison. For electrons in liquid xenon this ratio is decreasing with increasing field up to approximately 1 Td, due to the rising rates for elastic scattering in this field region. However, this ratio is increasing at higher fields due to the reduction of the rate for elastic scattering of high energy electrons. The E/n_0 dependence of this ratio is different for electrons in gases at low electric fields. For the values of E/n_0 lower than 10^{-2} Td this ratio is constant in the gas phase as the mean energy of electrons is very close to the thermal values. There is a narrow range of the reduced electric field between approximately 10^{-2} and 2×10^{-2} Td in which this ratio is rising with increasing field, due to the influence of the Ramsauer–Townsend minimum. At higher fields the qualitative trend of behavior of D_L/D_T is the same for electrons in liquid and gaseous xenon though the minimum is more pronounced in the liquid phase.

4.2. Streamer calculations

In our fluid simulations, we follow the transition of an electron avalanche into a negative streamer as well as the subsequent propagation of this streamer. The initial condition for both electrons and positive holes is a Gaussian distribution which is given by

$$n_e(x, 0) = \frac{300}{0.05\pi R_0^2 \frac{l}{3}\sqrt{2\pi}} \exp\left(-\frac{(x - 0.95l)^2}{2\left(0.05\frac{l}{3}\right)^2}\right). \quad (10)$$

This Gaussian is positioned near the cathode. It should be noted that the initial number densities of electrons and positive holes are selected so that the space charge effects are negligible. The values of l and R_0 are set to 5×10^{-5} m and 1×10^{-5} m respectively. The particular value of R_0 is chosen as an educated guess taking into account the initial distribution width and the spreading due to transverse diffusion. This value is in a good agreement with the values evaluated by the other authors [50, 51]. The length of the system l is determined by the requirement that the streamer velocity relaxes to a stationary value. The number of spatial cells used in our fluid simulations is 25000.

In figures 13 and 14 we show the formation and propagation of a negative streamer, assuming cases 1 and 4 for representing the inelastic energy losses, under the influence of the externally applied electric fields of 59 Td and 100 Td, respectively. For $E/n_0 = 59$ Td the difference between the ionization coefficients for liquid phase and rescaled gas is much higher than for $E/n_0 = 100$ Td. The simulations in the liquid phase are augmented by the simulation in which the transport data for electrons in the gas phase are for the gas phase scaled to the liquid density. The general features of the streamer profiles in the liquid xenon are the same as those of the streamers in gases [95, 96]. However, the space and time scales of the streamer formation are reduced by about three orders of magnitude due to a much greater number density of the background atoms in the liquid phase. The electron number density has a sharp peak in the streamer head where the electric field is significantly enhanced by the space charge effects. However, the number density is greatly reduced in the streamer channel where the external electric field is significantly screened. The further reduction of the number density of electrons in the streamer channel with increasing distance from the streamer head is clearly evident in the streamer profiles. This reduction can be attributed to the recombination of electrons and positive holes [50, 51]. A similar decrease of the electron number density in the streamer channel is observed for streamers in electronegative gases [50, 51].

We observe that the streamer formation as well as streamer propagation are greatly reduced with an increase of the number of excitations which are included in the model. The number density of electrons in both the streamer head and the streamer channel is also reduced. It can also be seen that the transition from an electron avalanche into a streamer is much slower in the case of the rescaled gas than in the first and the fourth cases of the liquid phase. Comparing figures 13 and 14, we see that this difference is much more pronounced at 59 Td than at 100 Td. To be specific, at 59 Td the distribution of electrons modeled in the case of the rescaled gas is still in the avalanche phase at the time instant when the streamer in the liquid phase, assuming the first case of representing inelastic energy losses, crosses the entire length l. On the other hand, at 100 Td the streamer modeled in the case of the rescaled gas is almost completely formed by the time when the streamer modeled in the first case reaches the boundary of the system. However, the streamer velocity and the number density of electrons calculated in the rescaled gas case are well below those in the liquid phase, assuming both cases 1 and 4, even at 100 Td. The observed streamer properties may be understood by considering the differences

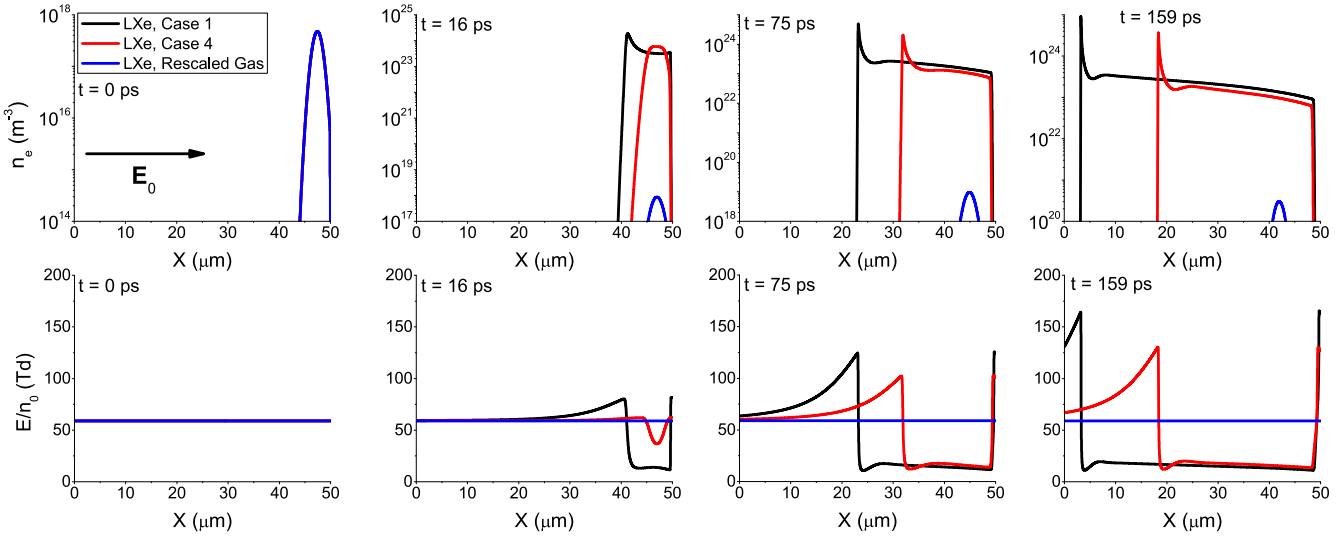

Figure 13. The formation and propagation of a negative streamer in liquid xenon for $E_0/n_0 = 59$ Td. The presented results are determined by assuming the first and the fourth cases for representing the inelastic energy losses. The results of streamer simulations obtained by using the gas phase transport properties which are scaled to liquid density are shown in the same figure for comparison. Here n_e refers to the electron number density, while E/n_0 refers to the reduced resultant electric field. The direction of the external electric field $\vec{E}_0$ is also shown in this figure.

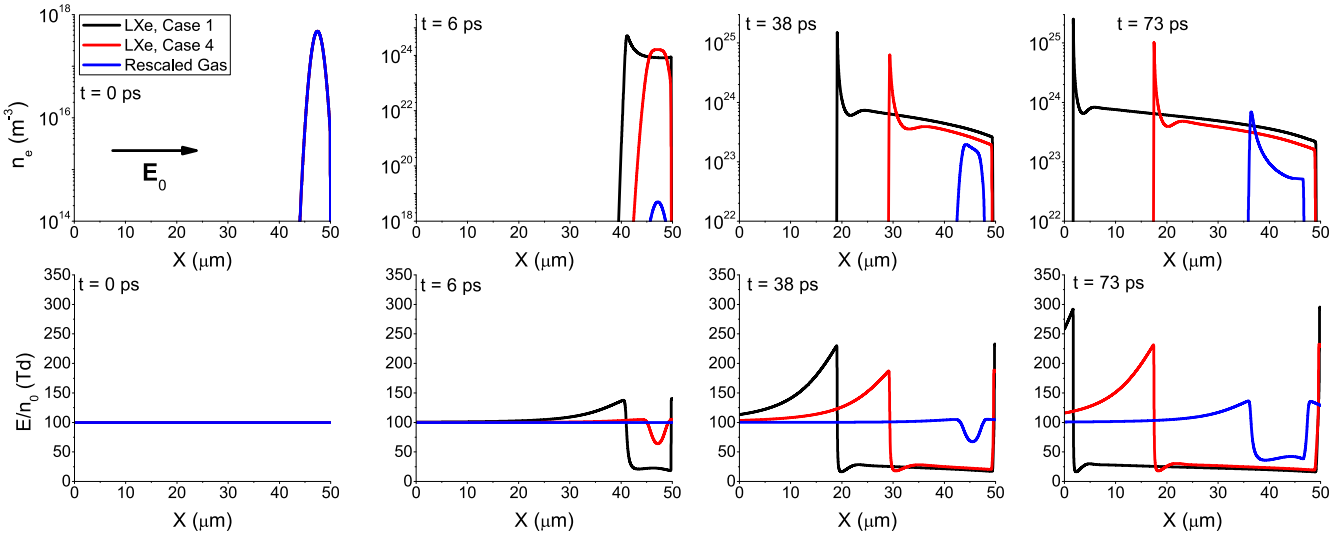

Figure 14. The formation and propagation of a negative streamer in liquid xenon for $E_0/n_0 = 100$ Td.

between the ionization coefficients in liquid and gaseous xenon. These differences are the most dominant at lower electric fields and gradually decrease with increasing field.

In figure 15 we show the profiles of negative streamers in liquid xenon for the applied reduced electric fields of 35 Td, 59 Td and 100 Td, respectively, at time 73 ps. The time instant of 73 ps has been carefully chosen since the fastest streamer in our simulations reaches the boundary of the system exactly at this time. The results are evaluated by considering all four cases for representing the inelastic energy losses. We observe that the number density of electrons in the streamer head and behind the ionization front in the streamer channel are decreased with the increase of the number of excitations in the model, independently of the applied electric field. It can also be seen that the number density of electrons and the streamer velocity increase with increasing E_0/n_0.

The streamer velocities determined by employing all four cases for representing the inelastic energy losses, are shown in figure 16 along with the streamer velocity calculated by using the gas phase transport properties which are scaled to liquid density. For comparison, the bulk drift velocity obtained in the first case, is shown in the same figure. It can be seen that the streamer velocity greatly exceeds the bulk drift velocity. This is expected, as the velocity of a negative streamer is determined by the combination of the electron velocity and the rate of the electron impact ionization in the streamer head, where the electric field is significantly enhanced, as well as by the strong diffusive fluxes in the streamer front. It can also be

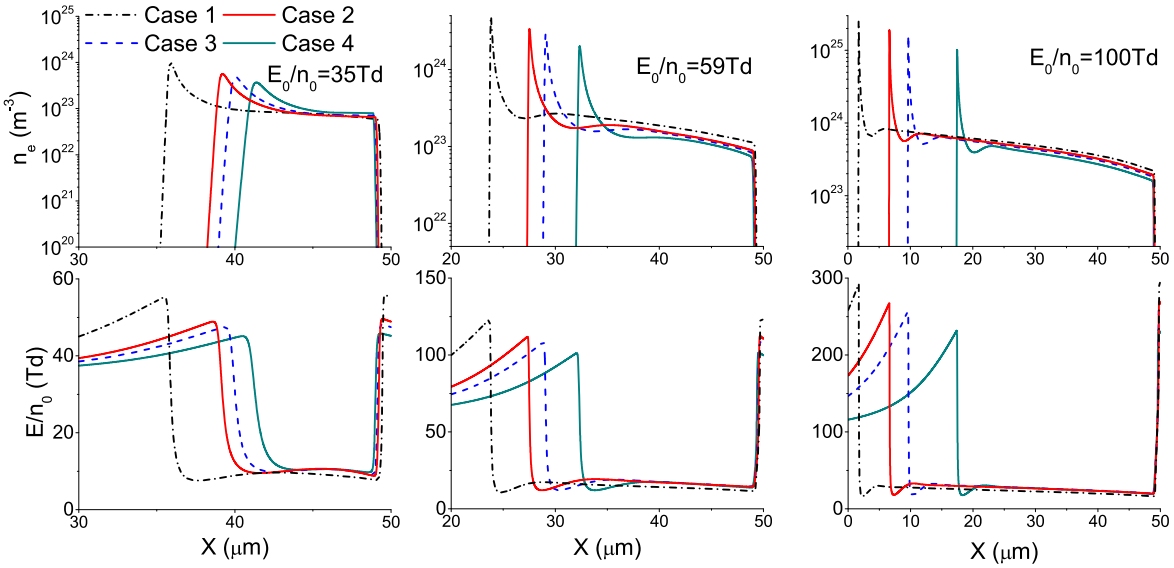

Figure 15. The spatial profiles of the electron number density n_e and the reduced electric field E/n_0 for three different values of the external electric field E_0. The displayed spatial profiles are determined by assuming all representations of the inelastic energy losses considered in the present work. All profiles are shown at 73 ps.

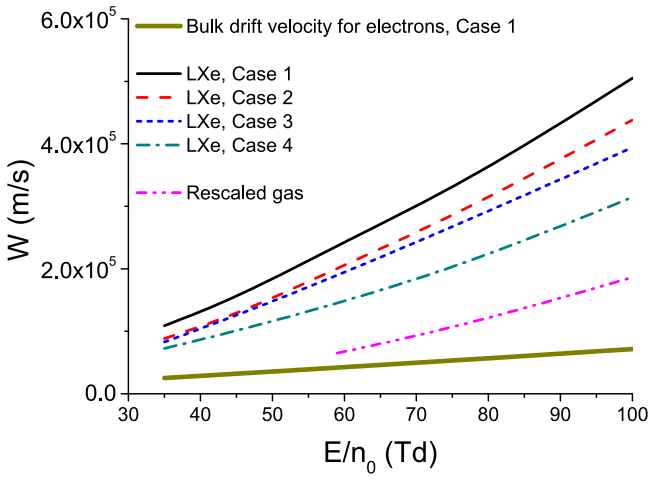

Figure 16. The streamer velocities calculated by assuming all representations of the inelastic energy losses considered in the present work. The streamer velocity obtained by using the gas phase transport data which is scaled to liquid density is displayed for comparison, as well as the bulk drift velocity of electrons, which is determined for the first case of representing the inelastic energy losses.

seen that the intensity of the streamer velocity determined in our fluid simulations strongly depends on the employed case for representing the inelastic energy losses in the liquid phase. The difference between the values of streamer velocities, which are obtained by assuming the first and the fourth cases, is about 40% at high electric fields. In addition, for the values of E_0/n_0 around 100 Td the streamer velocity determined by using the gas phase transport properties, which are scaled to liquid density, is about 2.5 times lower than the streamer velocity obtained in the first case for representing the inelastic energy losses. This difference is even more pronounced at lower electric fields. The differences between the calculated velocities of negative streamers are reflections of the corresponding differences between the first Townsend coefficient (see figure 9).

5. Conclusion

We have investigated the influence of the inelastic energy losses in liquid xenon on the transport properties of electrons and the dynamics of negative streamers, by using Monte Carlo simulations and the 1.5 dimensional fluid model. Four cases for representing the inelastic energy losses in liquid xenon are discussed in light of previous spectroscopy and photoconductivity experiments. These cases are employed for determining the transport properties of electrons by using Monte Carlo simulations. Our Monte Carlo code has been modified by including three effective scattering processes, which give a good representation of the coherent scattering of low energy electrons in non-polar liquids. The validity of our Monte Carlo code has been tested by calculating the mean energy, the drift velocity and the components of the diffusion tensor for electrons in the Percus Yevick model liquid. Our benchmark results for the Percus Yevick model are in an excellent agreement with those calculated by Tattersall *et al* [57]. We have determined the values of mean energy, drift velocity, diffusion tensor and the first Townsend coefficient for electrons in liquid xenon. Our results are in a good agreement with those of Boyle *et al* [34], as well as with the available experiments [56, 88, 89, 94]. However, since our calculations of transport properties span a range of the reduced electric field much wider than that investigated in experiments, one should be cautious to trust the calculated data outside the range covered in the experiments. This should be noted since we have approximated the cross sections for inelastic scattering and interband transitions of electrons in liquid xenon by using the cross sections for

electron scattering on an isolated xenon atom. In addition, we have neglected the electron phonon scattering, and we did not take into account the structure of the conduction band since we have approximated each electron by a free particle moving between individual collisions. It has been shown that there is a significant difference between the values of the first Townsend coefficient determined by employing different representations of the inelastic energy losses. The transport properties of electrons obtained in our Monte Carlo simulations, are used as input data in our simulations of the streamer dynamics. These simulations are based on the first order fluid model, and they follow the transition of an electron avalanche into a negative streamer and the subsequent streamer propagation. The results of these simulations strongly depend on the number of excitations which are included in the model. The intensity of the streamer velocity in the case in which all excitations are neglected exceeds the corresponding intensity in the case in which all excitations are included by about 40%, at high electric fields. This difference is in agreement with the difference in rates for ionization in these cases. Moreover, the value of the streamer velocity determined by using the transport properties from the gas phase, which are scaled to liquid density, is over 2.5 times lower than the streamer velocity calculated in the case in which all excitations are neglected. Furthermore, the speed of transition of an electron avalanche into a streamer in the rescaled gas phase is significantly lower than in the other cases investigated in our study. This difference is especially pronounced for the reduced electric fields lower than 100 Td. These results indicate that the correct representation of the elementary scattering processes in liquids is of crucial importance for the modeling of the electron transport and the electrical discharges in the liquid phase.

Our work concerning the modeling of electron transport in liquid xenon can be extended by employing *ab initio* cross sections for inelastic scattering and interband transitions in the liquid phase after these cross sections are determined. Further improvement of the model would be achieved by taking into account electron phonon scattering and trapping of electrons in density fluctuations as well as by going beyond the free electron approximation by considering the structure of the conduction band.

The extension of our streamer calculations by investigating the propagation of positive and negative streamers in a point to plane geometry and by taking into account nonlocality of the electron mean energy will be covered in future work. These calculations can be further generalized by considering the formation of gaseous filaments due to heating of the liquid, which is important on the nanosecond time scale.

Acknowledgments

This work was supported by the Grants No. OI171037 and III41011 from the Ministry of Education, Science and Technological Development of the Republic of Serbia and also by the project 155 of the Serbian Academy of Sciences and Arts. NG and RW acknowledge the financial support from the Australian Government, through the Australian Postgraduate Award, James Cook University, through the HDR Research Enhancement Scheme, and the Australian Research Council, through its Discovery and DECRA schemes.

ORCID iDs

I Simonović https://orcid.org/0000-0001-6704-9042
N A Garland https://orcid.org/0000-0003-0343-0199
D Bošnjaković https://orcid.org/0000-0002-2725-5287
Z Lj Petrović https://orcid.org/0000-0001-6569-9447
R D White https://orcid.org/0000-0001-5353-7440
S Dujko https://orcid.org/0000-0002-4544-9106

References

[1] Bruggeman P and Leys C 2009 *J. Phys. D: Appl. Phys.* **42** 053001
[2] Bruggeman P J *et al* 2016 *Plasma Sources Sci. Technol.* **25** 053002
[3] Fridman A and Friedman G 2012 *Plasma Medicine* (New York: Wiley)
[4] Kong M G, Kroesen G, Morfill G, Nosenko T, Shimizu T, van Djik J and Zimmermann J L 2009 *New J. Phys.* **11** 115012
[5] Jiang B, Zheng J, Qiu S, Wu M, Zhang Q, Yan Z and Xue Q 2014 *Chem. Eng. J.* **236** 348–68
[6] Malik M A, Ghaffar A and Malik S A 2001 *Plasma Sources Sci. Technol.* **10** 82
[7] Škoro N, Puač N, Živković S, Krstić-Milosević D, Cvelbar U, Malović G and Petrović Z L 2018 *Eur. Phys. J.* D **72** 2
[8] Puač N, Škoro N, Spasić K, Živković S, Milutinović M, Malović G and Petrović Z L 2017 *Plasma Process. Polym.* **15** e1700082
[9] Rond C, Desse J M, Fagnon J M, Aubert X, Er M, Vega A and Duten X 2018 *J. Phys. D: Appl. Phys.* **51** 335201
[10] Naidis G V 2015 *J. Phys. D: Appl. Phys.* **48** 195203
[11] Ushakov V Y, Klimkin V F and Korobeynikov S M 2007 *Impulse Breakdown of Liquids* (Berlin: Springer)
[12] Regenfus C and (The ArDM Collaboration) 2010 *J. Phys.: Conf. Ser.* **203** 012024
[13] Aprile E, Mukherjee R and Suzuki M 1990 *IEEE Trans. Nucl. Sci.* **37** 553
[14] Aprile E and Doke T 2010 *Rev. Mod. Phys.* **82** 2053
[15] Okada H, Doke T, Kashiwagi T, Kikuchi J, Kobayashi M, Masuda K, Shibamura E, Suzuki S, Takashima T and Terasawa K 2000 *Nucl. Instrum. Methods Phys. Res.* A **451** 427
[16] Egorov V V, Miroshnichenko V P, Rodionov B U, Bolozdinja A I, Kalashnikov S D and Krivoshein V L 1983 *Nucl. Instrum. Methods Phys. Res.* A **205** 373
[17] Aprile E and Baudis L 2008 *Proc. Sci.* **IDM2008** 018
[18] Gaitskell R 2008 *Proc. Sci.* **IDM2008** 018
[19] Boyle G J, McEachran R P, Cocks D G and White R D 2015 *J. Chem. Phys.* **142** 154507
[20] Sakai Y 2007 *J. Phys. D: Appl. Phys.* **40** R441
[21] White R D, Robson R E, Dujko S, Nicoletopoulos P and Li B 2009 *J. Phys. D: Appl. Phys.* **42** 194001
[22] Petrović Z L, Dujko S, Marić D, Malović G, Nikitović Ž, Šašić O, Jovanović J, Stojanović V and Radmilović-Radjenović M 2009 *J. Phys. D: Appl. Phys.* **42** 194002
[23] Robson R E, White R D and Petrović Z L 2005 *Rev. Mod. Phys.* **77** 1303
[24] Lekner J 1967 *Phys. Rev.* **158** 130

[25] Cohen M H and Lekner J 1967 *Phys. Rev.* **158** 305
[26] Atrazhev V M and Iakubov I T 1981 *J. Phys.* C **14** 5139
[27] Atrazhev V M and Dmitriev E G 1985 *J. Phys.* C **18** 1205
[28] Atrazhev V M, Iakubov I T and Pogosov V V 1995 *Phys. Lett.* A **204** 393
[29] Atrazhev V M and Timoshkin I V 1996 *Phys. Rev.* B **54** 252
[30] Atrazhev V M and Timoshkin I V 1998 *IEEE Trans. Dielectr. Electr. Insul.* **5** 450
[31] Atrazhev V M, Berezhnov A V, Dunikov D O, Chernysheva I V, Dmitrenko V V and Kapralova G 2005 *Proc. IEEE Int. Conf. on Dielectric Liquids (ICDL 2005)* p 329
[32] Sakai Y, Nakamura S and Tagashira H 1985 *IEEE Trans. Electr. Insul.* **EI-20** 133
[33] Nakamura S, Sakai Y and Tagashira H 1986 *Chem. Phys. Lett.* **130** 551
[34] Boyle G J, McEachran R P, Cocks D G, Brunger M J, Buckman S J, Dujko S and White R D 2016 *J. Phys. D: Appl. Phys.* **49** 355201
[35] Milloy H B and Crompton R W 1977 *Aust. J. Phys.* **30** 51
[36] Borghesani A F and Lamp P 2011 *Plasma Sources Sci. Technol.* **20** 034001
[37] Borghesani A F 2014 *Eur. Phys. J.* D **68** 62
[38] Petrović Z L, O'Malley T F and Crompton R W 1995 *J. Phys.* B **28** 3309
[39] Atrazhev V M, Iakubov I T and Roldughin V I 1976 *J. Phys. D: Appl. Phys.* **9** 1735
[40] Jones H M and Kunhardt E E 1993 *Phys. Rev.* B **48** 9382
[41] Kunhardt E E 1991 *Phys. Rev.* B **44** 4235
[42] Hove L V 1954 *Phys. Rev.* **95** 249
[43] Boyle G J, White R D, Robson R E, Dujko S and Petrović Z L 2012 *New. J. Phys.* **14** 045011
[44] Garland N A, Cocks D G, Boyle G J, Dujko S and White R D 2017 *Plasma Sources Sci. Technol.* **26** 075003
[45] White R D *et al* 2018 *Plasma Sources Sci. Technol.* **27** 053001
[46] Garland N A, Boyle G J, Cocks D G and White R D 2018 *Plasma Sources Sci. Technol.* **27** 024002
[47] Naidis G V 2016 *J. Phys. D: Appl. Phys.* **49** 235208
[48] Babaeva N Y, Naidis G V, Tereshonok D V and Smirnov B M 2017 *J. Phys. D: Appl. Phys.* **50** 364001
[49] Tereshonok D V, Babaeva N Y, Naidis G V, Panov V A, Smirnov B M and Son E E 2018 *Plasma Sources Sci. Technol.* **27** 045005
[50] Babaeva N Y and Naidis G V 1999 *Proc. 13th Int. Conf. on Dielectric Liquids (ICDL 1999) (Nara, Japan, July 20-25)* p 437
[51] Babaeva N Y and Naidis G V 1999 *Tech. Phys. Lett.* **25** 91
[52] Babaeva N Y and Naidis G V 2001 *J. Electrost.* **53** 123
[53] Nakamura S, Sakai Y and Tagashira H 1987 *JIEE Japan* **A107** 543
[54] Hayashi M 2003 *Bibliography of Electron and Photon Cross sections with Atoms and Molecules Published in the 20th Century—Xenon (NIFS-DATA-79)*
[55] Pitchford L C *et al* 2013 *J. Phys. D: Appl. Phys.* **46** 334001
[56] Derenzo S E, Mast T S and Zaklad B 1974 *Phys. Rev.* A **9** 2582
[57] Tattersall W J, Cocks D G, Boyle G J, Buckman S J and White R D 2015 *Phys. Rev.* E **91** 043304
[58] Bartels A 1973 *Phys. Lett.* **44A** 403
[59] Allen N L and Prew B A 1970 *J. Phys.* B **3** 1113
[60] Beaglehole D 1965 *Phys. Rev. Lett.* **15** 551
[61] Asaf U and Steinberger I T 1971 *Phys. Lett.* **34A** 207
[62] Laporte P and Steinberger I T 1977 *Phys. Rev.* A **15** 2538
[63] Laporte P, Subtil J L, Asaf U, Steinberger I T and Wind S 1980 *Phys. Rev. Lett.* **45** 2138
[64] Raz B and Jortner J 1968 *J. Chem. Phys.* **49** 3318
[65] Raz B and Jortner J 1970 *Proc. R. Soc.* A **317** 113
[66] Reininger R, Asaf U, Steinberger I T, Saile V and Laporte P 1983 *Phys. Rev.* B **28** 3193
[67] Asaf U and Steinberger I T 1974 *Phys. Rev.* B **10** 4464
[68] Hayashi M 2014 Hayashi Database www.lxcat.net
[69] von Zdrojewski W 1980 *Z. Naturforsch.* **35a** 672
[70] Reininger R, Asaf U and Steinberger I T 1982 *Chem. Phys. Lett.* **90** 287
[71] Garland N A, Simonović I, Boyle G J, Cocks D G, Dujko S and White R D 2018 *Plasma Sources Sci. Technol.* **27** 105004
[72] Gordon E B *et al* 1994 *Chem. Phys. Lett.* **217** 605
[73] Schüssler A S *et al* 2000 *Appl. Phys. Lett.* **77** 2786
[74] Gordon E B and Shestakov A F 2001 *Low Temp. Phys.* **27** 883
[75] Kunhardt E E, Christophorou L G and Luessen L H 1988 *The Liquid State and its Electrical Properties* (New York: Plenum) p 235
[76] Dujko S, Raspopović Z M and Petrović Z L 2005 *J. Phys. D: Appl. Phys.* **38** 2952
[77] Dujko S, White R D, Ness K F, Petrović Z L and Robson R E 2006 *J. Phys. D: Appl. Phys.* **39** 4788
[78] Dujko S, Raspopović Z M and Petrović Z L 2008 *J. Phys. D: Appl. Phys.* **41** 245205
[79] Perram J W 1975 *Mol. Phys.* **30** 1505
[80] Verlet L and Weis J J 1972 *Phys. Rev.* A **5** 939
[81] White R D and Robson R E 2011 *Phys. Rev.* E **84** 031125
[82] White R D and Robson R E 2009 *Phys. Rev. Lett.* **102** 230602
[83] Davies A J, Evans C J and Jones F L 1964 *Proc. R. Soc.* A **281** 164
[84] Bošnjaković D, Petrović Z L and Dujko S 2016 *J. Phys. D: Appl. Phys.* **49** 405201
[85] Hilt O and Schmidt W F 1994 *Chem. Phys.* **183** 147
[86] Hilt O and Schmidt W F 1994 *J. Phys. Condens. Matter* **6** L735
[87] Robson R E and Ness K F 1988 *J. Chem. Phys.* **89** 4815
[88] Miller L S, Howe S and Spear W E 1968 *Phys. Rev.* **166** 871
[89] Huang S S S and Freeman G R 1978 *J. Chem. Phys.* **47** 1355
[90] Petrović Z L, Crompton R W and Haddad G N 1984 *Aust. J. Phys.* **37** 23
[91] Robson R E 1984 *Aust. J. Phys.* **37** 35
[92] Vrhovac S B and Petrović Z L 1996 *Phys. Rev.* E **53** 4012
[93] Dujko S, White R D and Petrović Z L 2008 *J. Phys. D: Appl. Phys.* **41** 245205
[94] Shibamura E, Masuda K and Doke T 1984 *Proc. 8th Workshop on Electron Swarms*
[95] Li C, Brok W J M, Ebert U and Mullen J J A M 2007 *J. Appl. Phys.* **101** 123305
[96] Li C, Ebert U and Hundsdorfer W 2010 *J. Comput. Phys.* **229** 200